Climate Dynamics (2018) 51:4287–4307
https://doi.org/10.1007/s00382-017-4042-x

Diurnal variations of summer precipitation over the regions east to Tibetan Plateau

Yang Wu[1] · Anning Huang[1] · Danqing Huang[1] · Fei Chen[2] · Ben Yang[1] · Yang Zhou[3] · Dexian Fang[4] · Lujun Zhang[1] · Lijuan Wen[5]

Received: 27 April 2017 / Accepted: 4 December 2017 / Published online: 26 December 2017

Abstract
Based on the hourly gauge-satellite merged precipitation product with the horizontal resolution of 0.1° latitude/longitude during 2008–2014, diurnal variations of the summer precipitation amount (PA), frequency (PF), and intensity (PI) with different duration time over the regions east to Tibetan Plateau have been systematically revealed in this study. Results indicate that the eight typical precipitation diurnal patterns identified by the cluster analysis display pronounced regional features among the plateaus, basins, plains, hilly and coastal areas. The precipitation diurnal cycles are significantly affected by the sub-grid terrain fluctuations. The PA, PF and PI of the total rainfall show much more pronounced double diurnal peaks with the sub-grid topography standard deviation (SD) decreased. Meanwhile, the diurnal peaks of PA and PF (PI) strengthen (weaken) with the sub-grid topography SD enhanced. Over the elevated mountain ranges, southeastern hilly and coastal regions, the PA and PF diurnal patterns of the total rainfall generally show predominant late-afternoon peaks, which are closely associated with the short-duration ($\leqslant 3$ h) rainfall. Along the Tibetan Plateau to its downstream, the diurnal peaks of PA, PF and PI for the total rainfall all exhibit obvious eastward phase time delay mainly due to the diurnal evolutions of long-duration (> 6 h) rainfall. However, the 4–6 h rainfall leads to the eastward phase time delay of the total rainfall along the Taihang Mountains to its downstream. Further mechanism analysis suggests that the midnight to morning diurnal evolution of the long-duration rainfall is closely associated with the diurnal variations of the upward branches of thermally driven mountain-plain solenoids and the water vapor transport associated with the accelerated nocturnal southwesterly winds. The late-afternoon peak of the short-duration PA over the southeastern hilly and coastal regions is ascribed to the strong local thermal convections due to the solar heating in afternoon, while the early-evening peak of the short-duration PA over the elevated mountain ranges is significantly contributed by the upward warm-moist wind from the surrounding low-lying basins or plains.

1 Introduction

Diurnal variation of precipitation, as a response to the evolution of synoptic and climatic systems and local forcing, is an important aspect of the local climate and takes a significant feedback on certain thermal and dynamical conditions (Sorooshain et al. 2002). Due to the inhomogeneous

This paper is a contribution to the special issue on East Asian Climate under Global Warming: Understanding and Projection, consisting of papers from the East Asian Climate (EAC) community and the 13th EAC International Workshop in Beijing, China on 24–25 March 2016, and coordinated by Jianping Li, Huang-Hsiung Hsu, Wei-Chyung Wang, Kyung-Ja Ha, Tim Li, and Akio Kitoh.

✉ Anning Huang
anhuang@nju.edu.cn

✉ Danqing Huang
huangdq@nju.edu.cn

[1] CMA-NJU Joint Laboratory for Climate Prediction Studies, School of Atmospheric Sciences, Nanjing University, No. 163 Xianlin Avenue, Nanjing 210046, Jiangsu, China

[2] Nanjing Institute of Environmental Sciences, Ministry of Environmental Protection, Nanjing 210042, China

[3] Collaborative Innovation Center on Forecast and Evaluation of Meteorological Disasters/Key Laboratory of Meteorological Disaster, Ministry of Education, Nanjing University of Information Science & Technology (NUIST), Nanjing 210044, China

[4] Chongqing Institute of Meteorology and Science, Chongqing 401147, China

[5] Key Laboratory of Land Surface Process and Climate Change in Cold and Arid Regions, Chinese Academy of Sciences, Lanzhou 730000, China

underlying surface, monsoon systems, western Pacific subtropical high, and the nocturnal low-level jet, precipitation diurnal cycles present distinct regional and seasonal characteristics (Higgins et al. 1997; Wang et al. 2000; Yang and Smith 2005; He and Zhang 2010). Revealing the spatiotemporal features of precipitation diurnal cycles are not only helpful to understand the physical processes in the rainfall formation but also necessary to evaluate and improve precipitation parameterization schemes in climate models (Betts and Jakob 2002; Dai and Trenberth 2004; Demott et al. 2007).

In recent years, with the rapid development of the hourly gauge observed and satellite retrieved precipitation dataset, diurnal variability of precipitation has been extensively examined over East Asia. Yu et al. (2007a) revealed that diurnal variations of summer precipitation exhibit considerable regional features among five regions in the contiguous China. Whereafter, Yu et al. (2007b) further demonstrated that precipitation diurnal features over the central eastern China during the warm season are quite different between the short-duration and long-duration rainfall. Generally, short-duration rainfall peaks in the late afternoon, which is closely related to the thermally driven convection induced by surface solar heating (Dai et al. 1999; Yuan et al. 2012), while long-duration rainfall usually peaks during the period from midnight to early morning. This may be explained by the interactions between the local atmospheric conditions and the large-scale background circulations (Zhuo et al. 2014; Yin et al. 2009), e.g. nocturnal radiative cooling at cloud top (Lin et al. 2000; Li et al. 2004, 2008), the evolution of mesoscale convective systems (Carbone et al. 2002; Nesbitt and Zipser 2003; Jiang et al. 2006), and the large-scale monsoon circulations (Chen et al. 2009b, 2010; Yuan et al. 2010). Moreover, Chen et al. (2010) pointed out that the nocturnal long-duration precipitation shows an eastward phase time delay along the Yangtze River Valley due to the diurnal clockwise rotation of the low-tropospheric circulation, especially the accelerated nocturnal southwesterly winds. This close diurnal-scale correlation between precipitation and wind fields was further validated by Chen et al. (2012a, b) and Yuan et al. (2014a).

The regions east to the Tibetan Plateau (20–40°N, 110–125°E) is characterized by complex terrain, which consists of highly different landscapes including the elevated plateaus, Sichuan Basin, Loess Plateau, Taihang and Qingling-Wushan Mountains, the North China and Jianghuai Plain, and southeastern hilly and coastal areas (Fig. 1). At a large scale, the eastern plain areas can be regarded as the 'valley' relative to the plateaus in the west and as the land relative to the ocean in the east (Yu et al. 2014). Hence, precipitation diurnal variations over the regions east to the Tibetan Plateau are significantly influenced by the large-scale mountain-valley winds and land-sea breeze (Wu et al. 2007; Huang et al. 2010a, b; Yuan et al. 2012). Meanwhile, it is also of great sense to reveal the distinct regional and local topographic impacts on precipitation diurnal variations over the plateaus, valleys, mountainous, inland hilly and plain regions east to the Tibetan Plateau. Although many previous studies have made some progress in revealing the observed rainfall features over eastern China, most studies mainly focused on PA and scarcely discuss the features of the precipitation intensity (PI) and frequency (PF) with different duration time. Moreover, subject to the limited numbers of meteorological stations or the relatively coarse resolution of satellite data, the regional and local features of the precipitation diurnal cycles affected by complex topography have not been revealed in detail. In this study, we utilize the gauge-satellite merged precipitation product with very high temporal (hourly) and spatial resolutions ($0.1° \times 0.1°$) to detect the diurnal variations of rainfall with different duration time over the regions east to the Tibetan Plateau. Revealing the detailed rainfall features corresponding to the terrain fluctuation can provide a useful observation basis for climate model verification.

The rest of this paper is organized as follows. The data and methods are described in Sect. 2. The spatiotemporal distributions of PA, PF and PI diurnal peaks of precipitation with different duration time are compared in Sect. 3.1. Section 3.2 presents the spatial distributions of eight typical PA, PF and PI diurnal patterns based on the cluster analysis. The regional features of the diurnal variations in precipitation with different duration time and the associated atmospheric circulations are discussed in Sect. 3.3. Finally, the summary and discussions are given in Sect. 4.

2 2. Data and methods

2.1 Data

The precipitation dataset used in this study is the hourly, $0.1° \times 0.1°$, gauge-satellite merged precipitation product during 2008–2014, which can be obtained from the National Meteorological Information Center of China (available at http://data.cma.cn/search/keywords.html). This product is developed through a two-step merging algorithm of probability density function-optimal interpolation (PDF-OI) methods (Yu et al. 2013; Pan et al. 2012) by combining the quality-controlled rain gauge precipitation records at more than 30,000 automatic weather stations (AWS) with the Climate Precipitation Center Morphing (CMORPH) satellite precipitation estimates (Joyce et al. 2004). Hence, this gauge-satellite merged precipitation product synthesizes the advantages of gauge observed and satellite retrieved precipitation datasets. Compared to the previous limited and sparsely distributed hourly rain-gauge records or 3-h, $0.25° \times 0.25°$

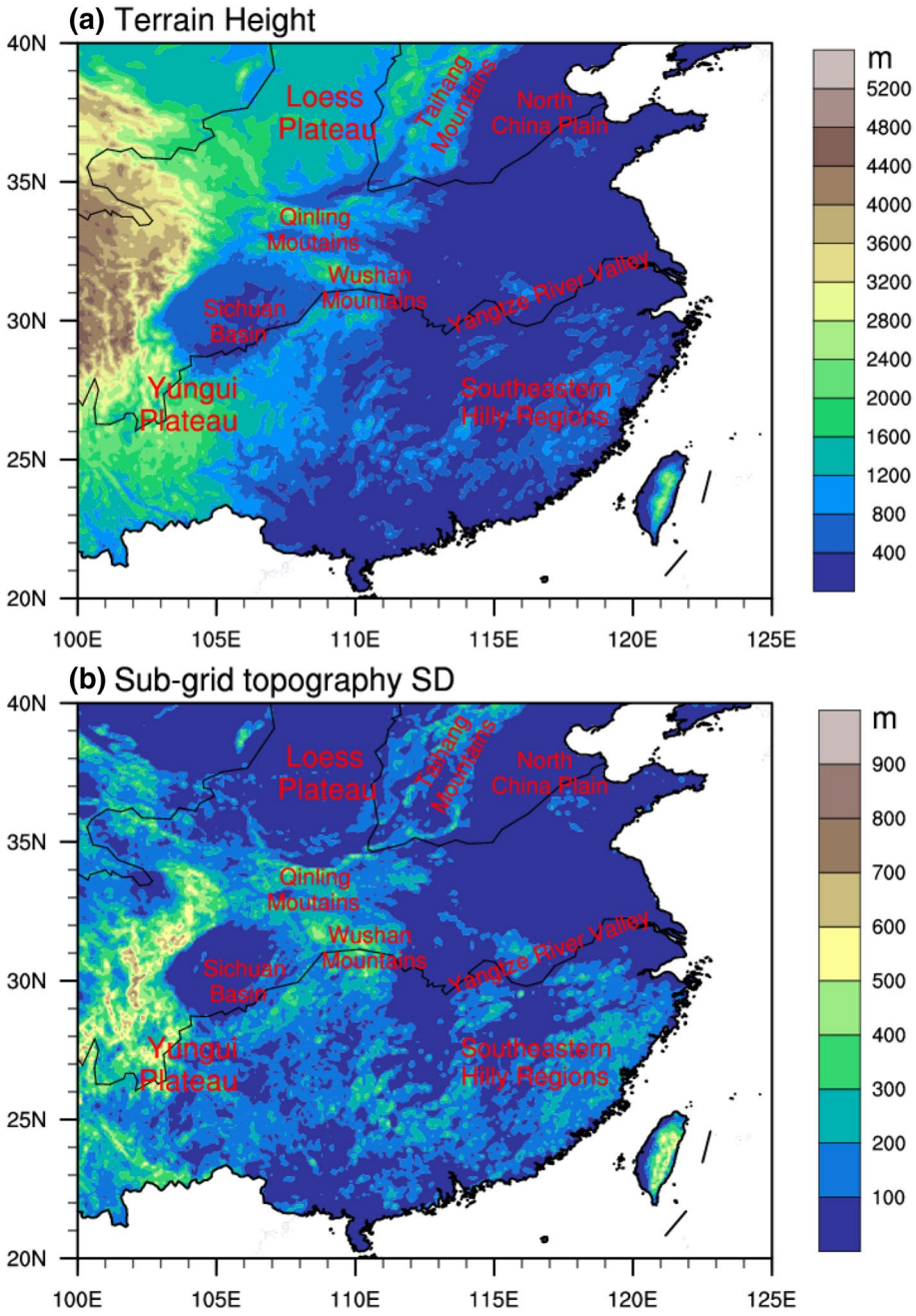

Fig. 1 Spatial distributions of **a** terrain height (m) and **b** sub-grid topography standard deviation (m) over the regions east to Tibetan Plateau. The Yangtze River and Yellow River are indicated by the dark curve lines

TRMM3B42 dataset, it provides a better opportunity for revealing the much more detailed spatiotemporal variations of rainfall with different duration time. The cross-validation results obtained by Shen et al. (2013, 2014) further indicate that this hourly precipitation product with 0.1° × 0.1° horizontal resolution shows much smaller systematic and random biases, root mean square errors and higher spatial correlation compared with both the AWS or CMORPH data and original PDF-OI derived precipitation product. Moreover, this dataset also shows good performance in capturing the varying features of hourly precipitation in heavy weather events over China.

The other datasets adopted in this study are listed as follows: (1) the ERA Interim data during 2008–2014 with the horizontal resolution of 0.25° at 00UTC, 06UTC, 12UTC and 18UTC (http://apps.ecmwf.int/datasets/data/interim-full-daily/). Variables used in current study include zonal wind (u), meridional wind (v), vertical velocity (w) and specific humidity (q) at 27 pressure levels ranging from 1000 to 100 hPa. (2) The Global Topographic Elevation data (GTOPO30) with a horizontal resolution of 30 s (~ 1 km) (available at the website https://lta.cr.usgs.gov/GTOPO30).

2.2 Methods

In this study, the total rainfall amount, frequency and intensity during summer are calculated by adopting a threshold of 0.1 mm h^{-1} for each hour of a day at each grid box (Dai et al. 1999). Subsequently, following Zhou et al. (2008), the summer averages of precipitation amount (PA, the accumulated measurable precipitation divided by the total hours in summer), frequency (PF, the percentage of total precipitating hours with the measurable precipitation $\geqslant$ 0.1 mm h^{-1} to the total hours in summer), and intensity (PI, the accumulated measurable precipitation averaged over the total precipitating hours with the measurable precipitation $\geqslant$ 0.1 mm h^{-1} in summer) during 2008–2014 for each hour of a day at each grid are obtained. In addition, the number of hours between the start and the end of an event without any intermittence during which the rainfall is less than 0.1 mm h^{-1} are regarded as the duration time (Yu et al. 2007b). Based on different duration time, we further define the long-duration (> 6 h) and short-duration ($\leqslant$ 3 h) rainfall events (Yu et al. 2007b; Li et al. 2008).

To compare the rainfall events with different duration time over different regions, the diurnal variations of PA, PF and PI are normalized by the their daily mean according to $D(h) = (R(h) - R_m)/R_m$ (Yu et al. 2007b), where h ranging from 0 to 23 indicates the Beijing Time (BJT). $R_m = \frac{1}{24}\sum_{h=0}^{h=23} R(h)$ is the daily mean of PA, PF and PI.

In addition, we adopted the harmonic analysis (Angelis et al. 2004; Roy and Balling 2005; Yin et al. 2009; Zhang et al. 2017) on the normalized 24-h time series of PA, PF and PI The first three harmonic components are retained to represent the precipitation diurnal cycle and given by:

$$\hat{P}(h) = \overline{P} + \sum_{m=1}^{m=3} C_m \cos\left(\frac{2k\pi}{24} - \sigma_m\right) + residual \tag{1}$$

$$e_m = \frac{0.5C_m^2}{P_{\text{var}}} \tag{2}$$

$$F_m = \frac{0.5C_m^2 \times (24-2-1)}{(P_{\text{var}} - C_m^2) \times 2} \tag{3}$$

where $\hat{P}(h)$ is the estimate of PA, PF and PI in each hourly interval, $h = 1, 2, \ldots, 24$ indicates BJT expressed by the hour of a day ranging from 00:00 to 23:00 BJT. $\overline{P}$ is the daily mean value. m ranging from 1 to 3 denotes the first three harmonics. The *residual* is the higher order harmonics of precipitation diurnal variations. C_m is the amplitude and σ_m is the phase for the m_{th} harmonic. P_{var} represents the variance of the 24-h PA, PF and PI time series. e_m indicates the contribution of the m_{th} harmonic to the total daily variance and is used to reveal how much of the diurnal variations can be explained by the m_{th} harmonic. F_m can be obtained according to Eq. (3). The F-test is used to determine the significance of the harmonics by comparing F_m with the inverse of the F distribution function with 2 and 21 degrees of freedom at significance level of 90% (Benedetto 1996; Yin et al. 2009). The purposes of the harmonic analysis are not only to obtain the valid data size but also to improve the statistical significance for the cluster analysis (Fujibe 1999).

Different from the other cluster methods, the Fuzzy c mean cluster analysis, exhibits some advantages in obtaining a small number of representative patterns from the voluminous data (Fujibe 1989; Chen et al. 2009a; Zhang et al. 2017), allows for partial membership to all clusters and ascertains the major patterns by selecting the maximum memberships at grids. Following Zhang et al. (2017), if the sum of the first three harmonics contributes more than 70% to the total daily variance and at least one of the first three harmonics passes the statistical significance level of 90%, these data (diurnal cycles of PA, PF and PI) are picked out for the Fuzzy c mean cluster analysis (Fujibe 1989, 1999). Then, we conduct the cluster analysis on the normalized 24-h time series of PA, PF and PI for the rainfall with different duration time. The degrees of membership to the eight cluster centers are calculated based on the method in current study. According to the maximal partial memberships at grids, we can obtain the spatial distributions of eight typical patterns and synthesize the corresponding precipitation diurnal cycles at the grids belonging to a given cluster. Detailed descriptions of Fuzzy c mean cluster analysis can be found in Fujibe (1989, 1999). Meanwhile, the standard deviations of PA, PF and PI among the grids corresponding to a given cluster at each hour of day are used to show how the robustness of the cluster analysis is.

To reveal the relation between the spatial distribution of the gauge-satellite merged precipitation and that of the sub-grid terrain fluctuation which can be reflected by the sub-grid topography standard deviation (SD) (Fig. 1b) at each grid of the gauge-satellite precipitation data, based on the GTOPO30 terrain height with the horizontal resolution of 30 arc s, the sub-grid topography SD at a given grid (i, j) of the gauge-satellite merged precipitation can be calculated by:

$$SD(i,j) = \sqrt{\frac{1}{169}\sum_{i1,j1=-6}^{i1,j1=6} (h(i1,j1) - ah)^2} \tag{4}$$

where ah is the regional mean GTOPO30 terrain height in the region across the 169 points within the grid (i, j) of the gauge-satellite merged precipitation, $h(i1, j1)$ is the terrain height at the grid $(i1, j1)$ of the GTOPO30 data. $i1$ and $j1$ indicate the GTOPO30 grid number for the west–east

direction and south-north direction respectively. The resolution of the gauge-satellite precipitation is 0.1°, so the total grids of the GTOPO30 with the resolution of 30 arc seconds within the given grid (i, j) of the gauge-satellite precipitation should be 169 (13 by 13).

3 3. Results

3.1 Spatial distribution of the summer precipitation diurnal cycles

Figure 2 gives the spatial distributions of PA, PF and PI diurnal peaks (hereafter PPA, PPF and PPI) and their occurrence time. From Fig. 2a, the PPA of total rainfall with the intensity above 0.6 mm h^{-1} is located over the south peripheries of Yungui Plateau, eastern flanks of the Tibetan Plateau,

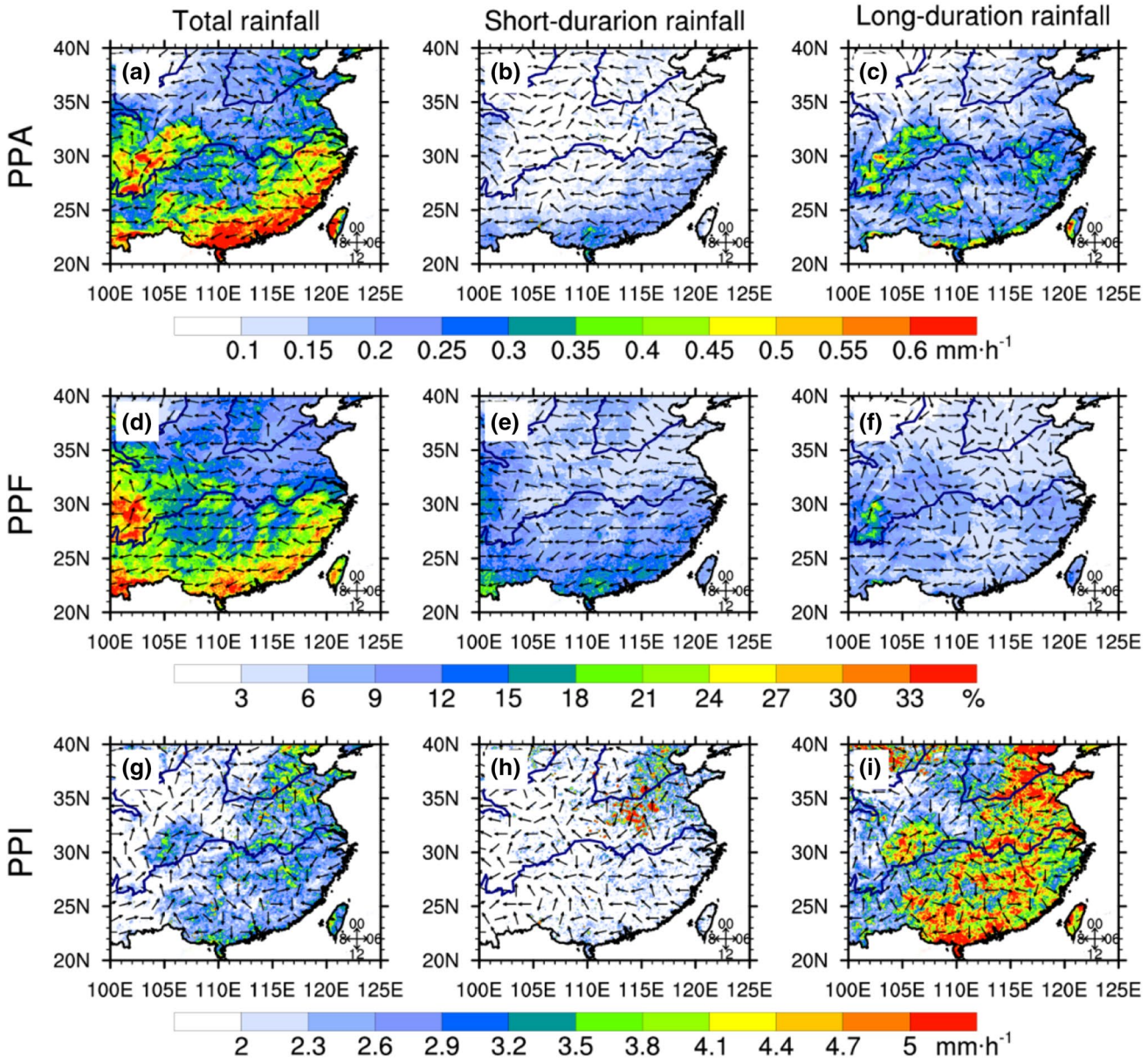

Fig. 2 Spatial distributions of the diurnal peaks (shadings) of the total (the left panel), short-duration (the middle panel), and long-duration (the right panel) precipitation amount, frequency and intensity in summer averaged over 2008–2014 and their occurrence time (arrows indicate BJT, see phase clock)

southeastern hilly and coastal regions, where the PPF of the total rainfall usually exceeds 30% (Fig. 2d). Over the southeastern hilly and coastal regions, the PA and PF of the total rainfall show coherent late-afternoon peaks (Fig. 2a, d), while they usually occur during midnight to early morning over the eastern peripheries of Tibetan Plateau to Sichuan Basin and some sub-regions in the North China Plain. Different from the distributions of the large PPA and PPF centers in Fig. 2a, d, the PPI of the total rainfall with the intensity above 3.2 mm h^{-1} is mainly situated in valleys, riparian, or coastal plains (Fig. 2g). This may be ascribed to the abundant moisture fluxes carried by the accelerated low-level southwesterly jet due to the boundary layer friction and decreased turbulent mixing at night (Higgins et al. 1997; Carbone and Tuttle 2008; He and Zhang 2010; Bao et al. 2011).

From Fig. 2b, the PPA of short-duration rainfall with the intensity exceeding 0.15 mm h^{-1} mainly occurs in the elevated mountainous regions, such as eastern peripheries of Tibetan and southeastern Yungui Plateau, and the southeastern hilly and coastal regions, where the PPF is usually more than 12% (Fig. 2e). The PA and PF of short-duration rainfall show a leading late-afternoon peak and usually occur earlier over southern regions than over northern regions. From Fig. 2b, e, h, although the PPF of the short-duration rainfall is below 6% in the North China Plain, the PPA is over 0.15 mm h^{-1} and greater than that over the Taihang Mountains due to the strong PPI exceeding 3.2 mm h^{-1}.

It is notable that the PPA, PPF and PPI of the long-duration rainfall all exhibit an obvious clockwise diurnal phase time delay along the eastern Tibetan Plateau peripheries to the middle-lower reaches of the Yangtze River Valley (Fig. 2c, f, i). In addition, the spatial correlation coefficients between the total rainfall and long-duration rainfall shown in Fig. 2 for the PPA, PPF and PPI are over 0.83 which is statistically significant at the 99% confidence level, indicating that the PPA, PPF and PPI of the total rainfall over most parts of the study region are mainly contributed by the long-duration rainfall in summer, this is consistent with the findings of Yu et al. (2007b).

3.2 Results of the cluster analysis

To give detailed typical patterns of the summer rainfall diurnal variations over the regions east to the Tibetan Plateau, we conducted the cluster analysis as described in Sect. 2.2 on the normalized 24-h time series of the PA, PF and PI for the total rainfall and the rainfall with different duration time, respectively. Figures 3, 4 and 5 show the eight typical diurnal patterns of PA, PF and PI for the total rainfall based on the Fuzzy c mean cluster analysis. The colored regions in Figs. 3a, 4a and 5a denote the first three harmonics passing the F test at 90% significant confidence level and jointly contributing more than 70% to the total daily variance. As implied in the red (black) lines derived from synthetic (original) data (Figs. 3b, 4b, 5b), the raw data can be well reflected by the harmonic analysis in all typical patterns.

From Fig. 3a, the PA diurnal patterns exhibit very distinct regional features. As shown in Fig. 3a, b, the rainfall with the typical diurnal patterns k = 6–8 over the Loess Plateau, Taihang Mountains, Qinling-Wushan Mountains, most southeastern Yungui Plateau, southeastern hilly and coastal regions peaks in late afternoon. This late-afternoon PPA is mainly attributed to the low-level atmospheric instability triggered by surface solar heating (Yuan et al. 2010; Luo et al. 2013). Specifically, the late-afternoon precipitation over the coastal regions in southern China is also related to the orographic lifting effect and more water vapor transported by the sea breeze during the monsoon break period (Yu et al. 2009; Yuan et al. 2012; Chen et al. 2014). Meanwhile, it can be noted that the PA diurnal cycles over most regions typically show eastward phase time delay, i.e., over the regions north to 35°N, the PA patterns k = 6–8 with late-afternoon (16:00–19:00 BJT) peaks over Loess Plateau and Taihang Mountains shift to the patterns k = 1–3 with early evening to early morning (20:00–06:00 BJT) peaks over the downstream plains. Over the areas between 26°N and 32°N, the PA patterns k = 1–5 with nocturnal to early-morning (00:00–08:00 BJT) peaks over the east peripheries of Tibetan and Yungui Plateau, and Sichuan Basin change to the PA patterns k = 6–8 with late-afternoon peaks over the hilly and coastal areas in the east. However, the PA diurnal cycles over the tropical regions located in the areas south to 24°N display very weak eastward phase time delay. Compared to the PA pattern k = 1, the diurnal peaks of the PA patterns k = 2–4 get strengthened during 04:00–08:00 BJT with a relatively larger value exceeding 0.30 mm h^{-1} over the downstream of highlands, such as Sichuan Basin and the North China Plain. This can be ascribed to the increased moisture supply carried by the nocturnal accelerated low-level southwesterly winds (Fig. 10a vs. b).

Compared to the PA of the total rainfall, the PF diurnal cycles of the total rainfall over most parts of eastern China can be well explained by the first three harmonics (80.52 versus 92.12%). Hence, we can observe a more pronounced regional distribution of PF patterns and corresponding rainfall diurnal cycles. The PF pattern k = 1 with an early-evening peak locates over the elevated mountainous regions of Taihang mountains and Tibetan Plateau. Compared with the distributions of PA patterns k = 2–4 for the total rainfall (Fig. 3), the PF patterns k = 2–4 for the total rainfall (Fig. 4) over the downstream of the Taihang mountains and patterns k = 2–5 over the eastern flanks of Tibetan and Yungui Plateau show more apparent eastward phase time delay features. Additionally, the diurnal peaks of the PF patterns k = 2–5 weaken gradually during 02:00–08:00

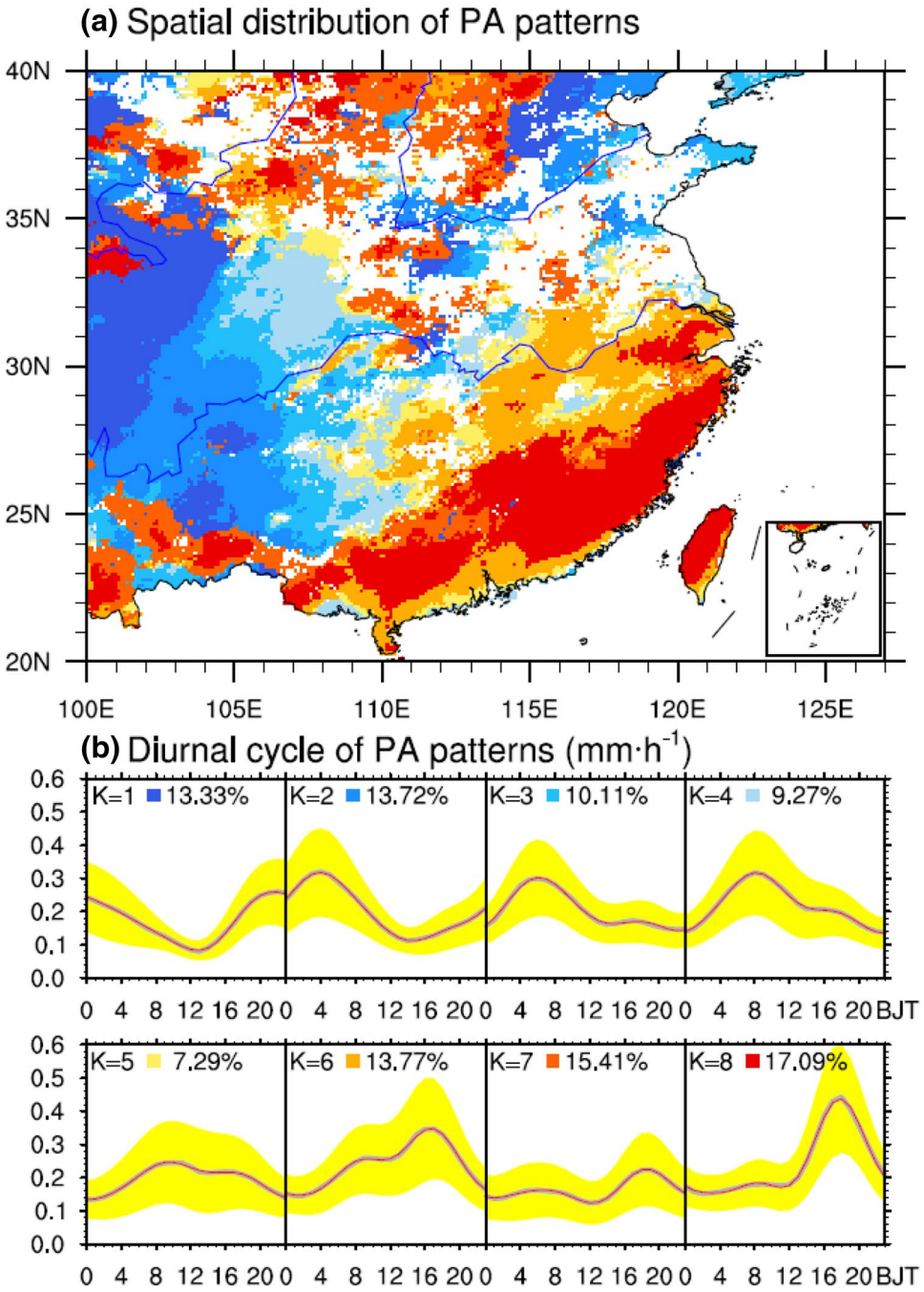

Fig. 3 **a** Spatial distributions of summer PA patterns and **b** corresponding diurnal cycles averaged over 2008–2014 along with the standard deviation of the PA among the grids belonging to a given cluster (shaded in yellow). The markers of patterns K in **a** are labeled at **b**, accompanied by the ratio to the colored region that can be well explained by the first three harmonics. The red (gray) lines show the diurnal cycles of PA with (without) Fourier analysis

BJT. The PF pattern k = 7 located over most Yangtze-Huai River Valley shows a weak early-morning peak and a relatively strong late-afternoon peak. The PF patterns k = 6 and 8 with strong late-afternoon peaks mainly located over the southeastern peripheries of Yungui Plateau, Loess Plateau, Wushan Mountains, southeastern hilly and coastal regions show relatively larger diurnal amplitude compared to the other PF diurnal patterns.

Different from PA and PF, the PI diurnal cycles of the total rainfall over approximate half of the study region cannot be appropriately depicted by the diurnal and semidiurnal cycles (Fig. 7a). Along the eastern peripheries of Tibetan Plateau to the downstream areas between 100°E and 110°E, the PI patterns k = 2–6 for the total rainfall show a midnight to early-morning phase time delay. Moreover, the PPI enhances gradually during 02:00–08:00 BJT. Over the regions east to 110oE, the PI pattern k = 7 is characterized by a morning peak, while the PI pattern k = 8 shows two comparable peaks around 10:00 and 18:00 BJT.

As the cluster analysis of the PF for the total rainfall can give a better clarity between different rainfall patterns compared to PA and PI mentioned above, Figs. 6, 7 and 8 further

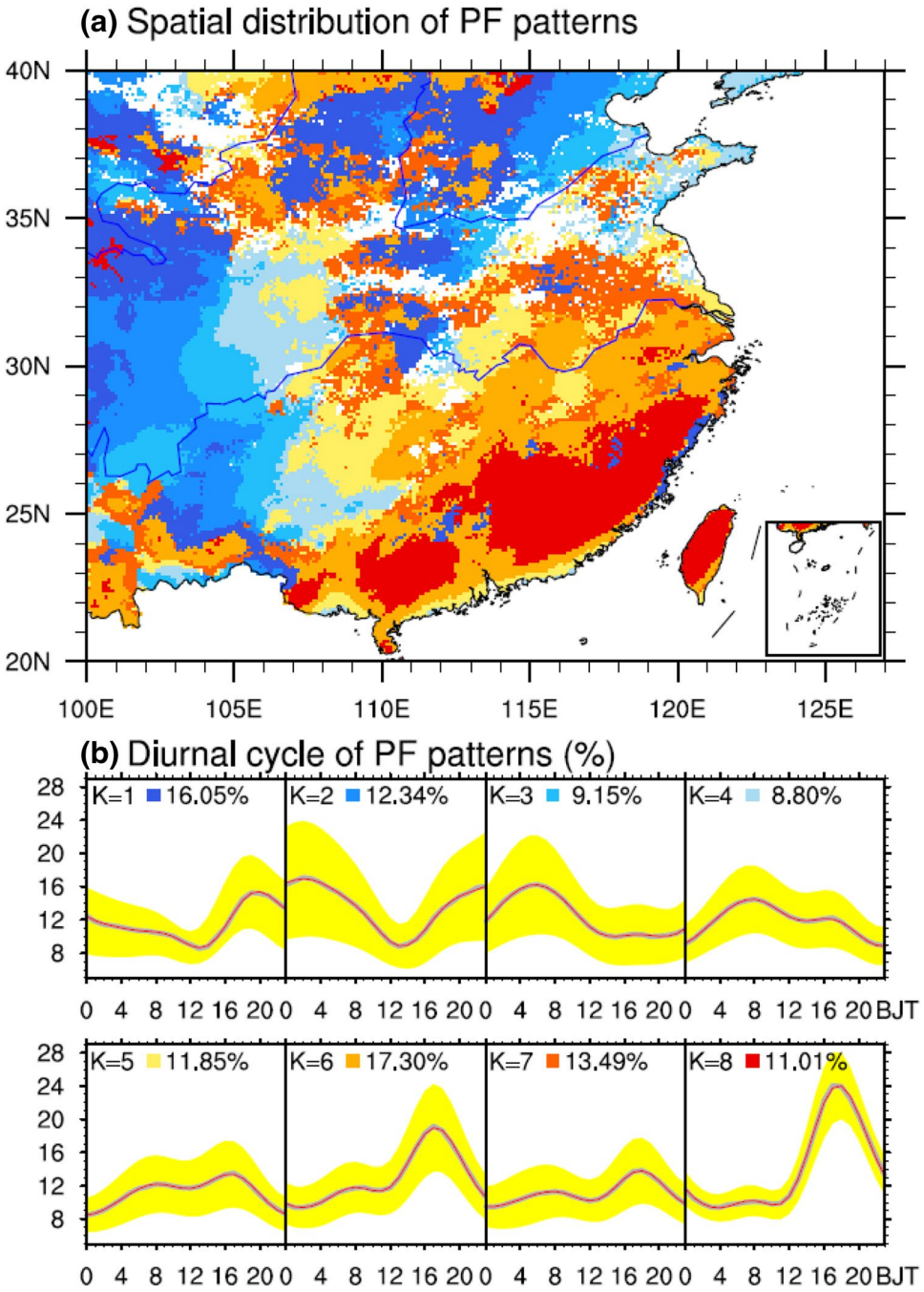

Fig. 4 Same as in Fig. 3, but for the PF of the total rainfall

give the cluster analysis results on the PF of the rainfall events with different duration time. From Fig. 6, the long-duration PF diurnal patterns k = 1–5 show clear eastward phase time delay during 02:00–08:00 BJT along the east peripheries of Tibetan Plateau to the downstream lowlands and the amplitude of the corresponding diurnal cycle weakens gradually, which is highly consistent with the spatiotemporal variations of the PF patterns k = 2–5 in the total rainfall (Fig. 4). However, the long-duration PF patterns k = 3–6 with early-morning peaks dominate the Taihang mountains and North China Plain, while the PF patterns k = 1–4 of the total rainfall over there show apparent eastward phase time delay in Fig. 4. Despite of the long duration time, the PF patterns k = 7 and 8 still show a very weak late-afternoon diurnal peak over the southeastern hilly and coastal regions. This is also in accord with the late-afternoon PPF of long-duration rainfall (Fig. 2f). From Fig. 7, the short-duration PF patterns k = 1–8 all show consistent late-afternoon diurnal peaks during 17:00–18:00 BJT. Specifically, the short-duration PF patterns k = 5–8 with diurnal peaks at 17:00 BJT mainly locate over the southeastern hilly and coastal regions, where the dominant mode is the PF pattern k = 8

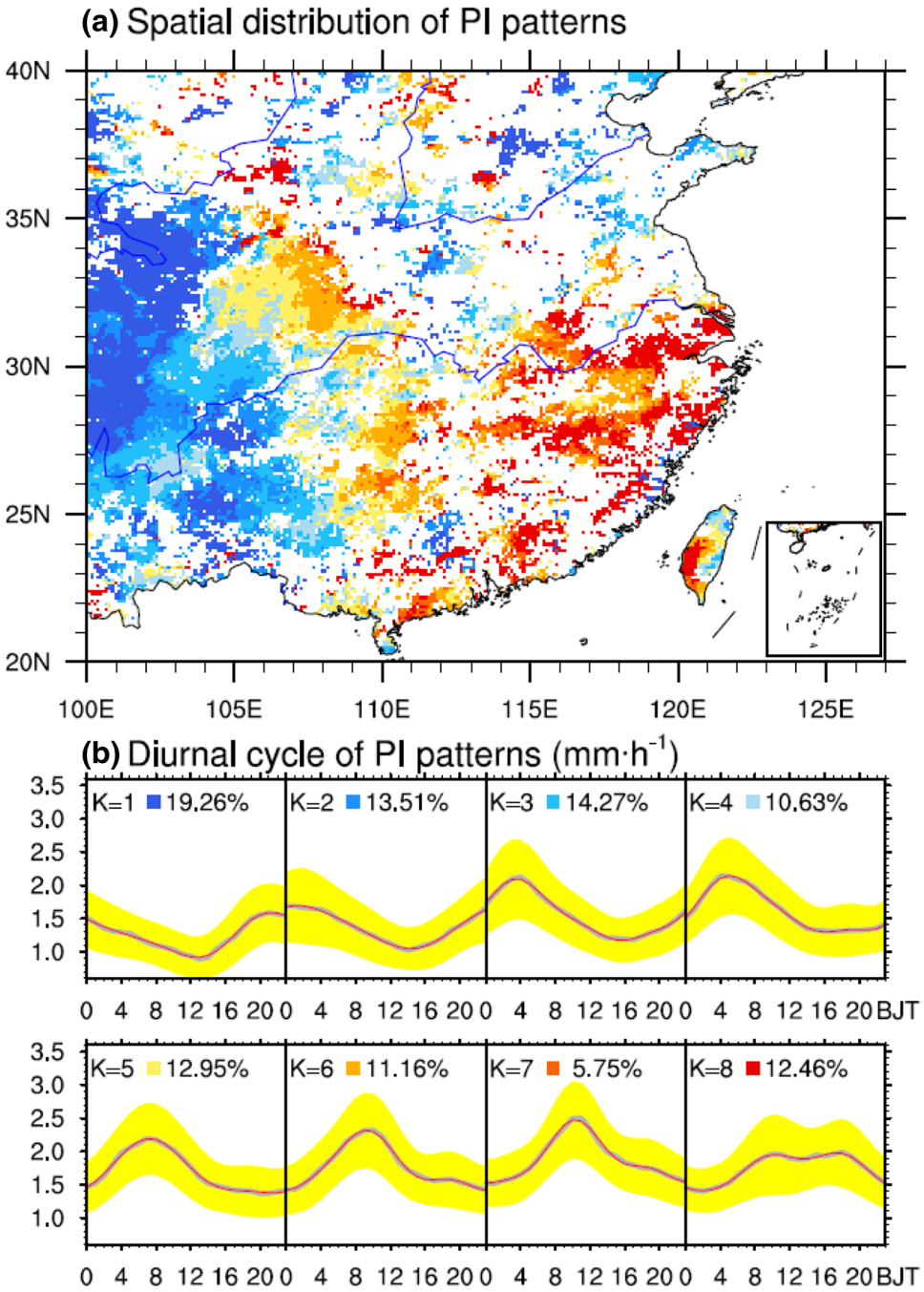

Fig. 5 Same as in Fig. 3, but for the PI of total rainfall

with a strong late-afternoon peak exceeding 11%. However, the short-duration PF patterns k = 1–4 mainly locate over the Loess Plateau, Taihang mountains, eastern peripheries of Tibetan and Yungui Plateau and usually peak at 18:00 BJT.

In the central northern China, Yuan et al. (2014b) regards the rainfall with the duration time ≤ 6 h as the crucial factor for the eastward propagation from Taihang mountains to North China Plain, ascribing it to the topographic modulation on the low-level temperature, moisture and wind fields. In this study, the short-duration PF patterns k = 1 and 2 with dominant late-afternoon peaks at 18:00 BJT are confined to the Taihang Mountains' ranges. Additionally, the PF patterns k = 3–5 of the long-duration rainfall exhibit early-morning peaks during 07:00–09:00 BJT over the North China Plain. No apparent eastward propagation can be found in both short-duration and long-duration rainfall to explain the eastward phase delay of the total rainfall diurnal peaks over there. Hence, we further give the cluster results on the PF of the rainfall with 4–6 h duration in Fig. 8. The midnight to early-morning PF patterns k = 1–4 share similar spatial distribution to the long-duration rainfall in the eastern peripheries of Tibetan and Yungui Plateau. However, along the

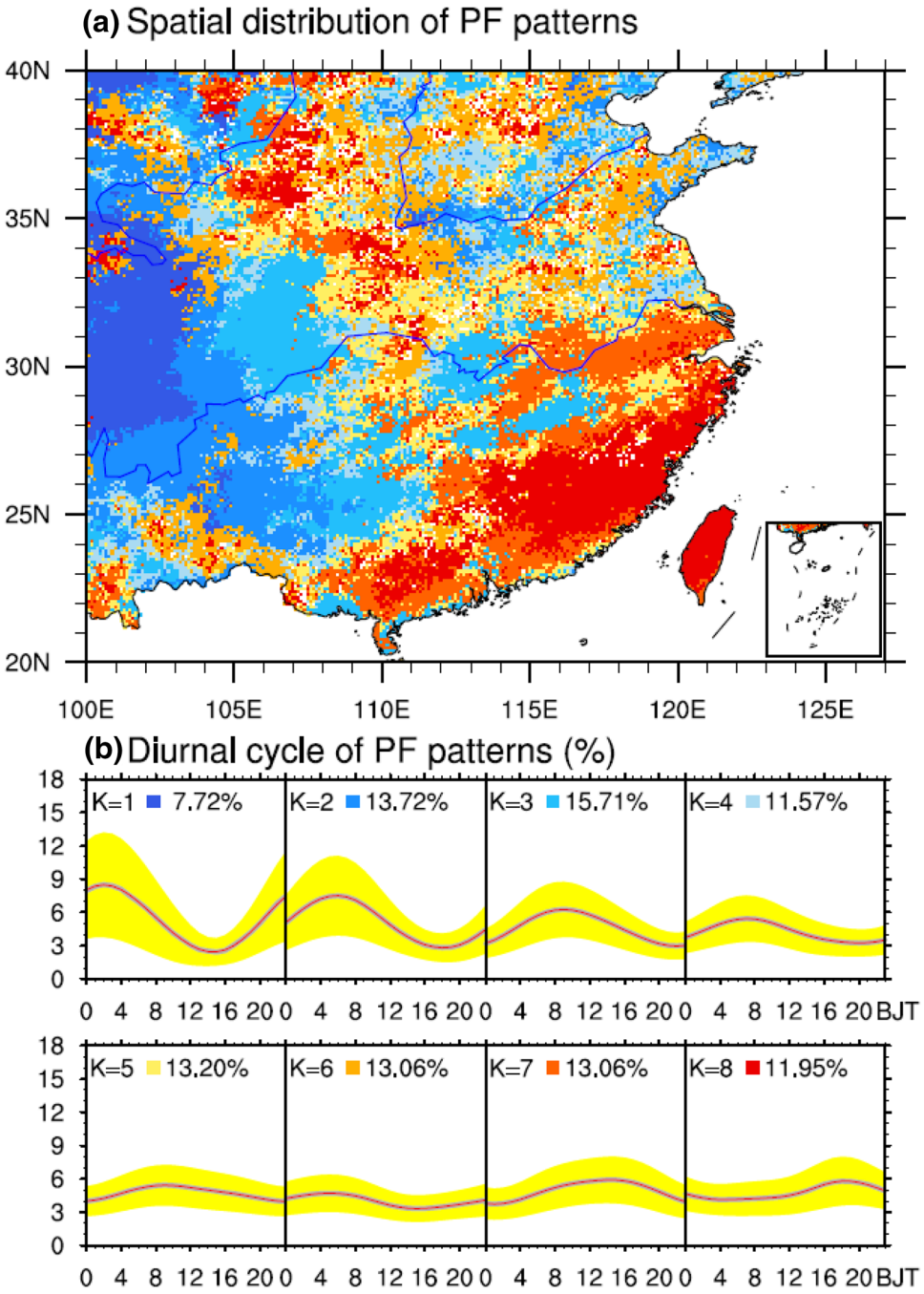

Fig. 6 Same as in Fig. 3, but for the PF with long-duration rainfall

Taihang mountains to the North China Plain, the PF patterns k = 1–4 for the 4–6 h rainfall lead to the eastward phase time delay in the PPF of the total rainfall. Over the southeastern hilly and coastal regions, the PF patterns k = 7 and 8 of the rainfall with the duration time of 4–6 h are characterized by a leading late-afternoon peak similar to those of the short-duration rainfall. These unique spatiotemporal features of the rainfall with 4–6 h duration are firstly shown by the cluster analysis and the fine-scale data.

According to the cluster analysis mentioned above, the spatial patterns of PA, PF and PI for the rainfall with different duration time vary regionally among plateaus, basins, plains, hilly and coastal areas. To detect the relations between the PA, PF and PI patterns with the sub-grid topography fluctuations, we further give the diurnal precipitation cycles varying with different sub-grid topography SD in Fig. 9. The PA and PF diurnal cycles of the total rainfall with the sub-grid topography SD below 200 m show a weak early-morning peak and a relatively larger late-afternoon peak at 17:00–19:00 BJT (Fig. 9d, h). This late-afternoon PPA and PPF of the total rainfall is mainly contributed by the short-duration rainfall in Fig. 9a, e. With

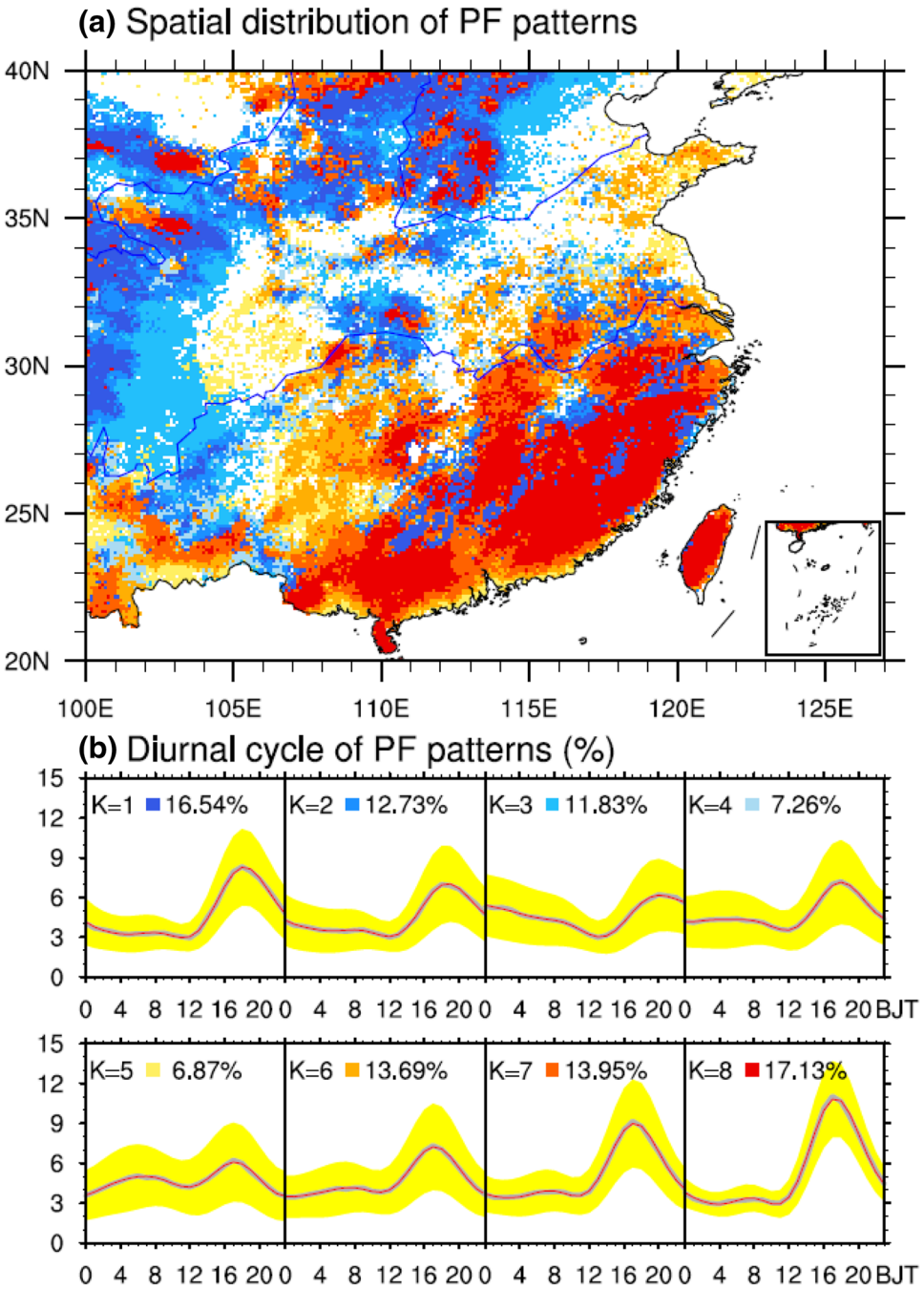

Fig. 7 Same as in Fig. 3, but for the PF with short-duration rainfall

the sub-grid topography SD increased from 200 to 700 m, the early-morning PPA and PPF of the total rainfall enhance gradually and change to strong midnight to early-morning type, which is similar to the sub-grid topography SD-time variations of the long-duration rainfall between 00:00–09:00 BJT in Fig. 9c, g. From Fig. 9k, l, the PI of the total and long-duration rainfall show a weak late-afternoon peak and a strong midnight to early-morning peak. While the PI of the short-duration and 4–6 h rainfall exhibit a much stronger late-afternoon peak (Fig. 9i, j), indicating that the midnight to early-morning PI peaks in the total rainfall mainly result from those of the long-duration rainfall. Overall, the sub-grid terrain fluctuations show significant impacts on the precipitation diurnal cycles. With the sub-grid topography standard deviation (SD) decreased, the PA, PF and PI of the total rainfall tend to show much more pronounced double diurnal peaks. Meanwhile, the diurnal peaks of PA and PF (PI) strengthen (weaken) with the sub-grid topography SD enhanced.

To indicate the overall precipitation diurnal evolution features over eastern China in summer, Fig. 10 further gives the spatial distribution of the climatic mean PA

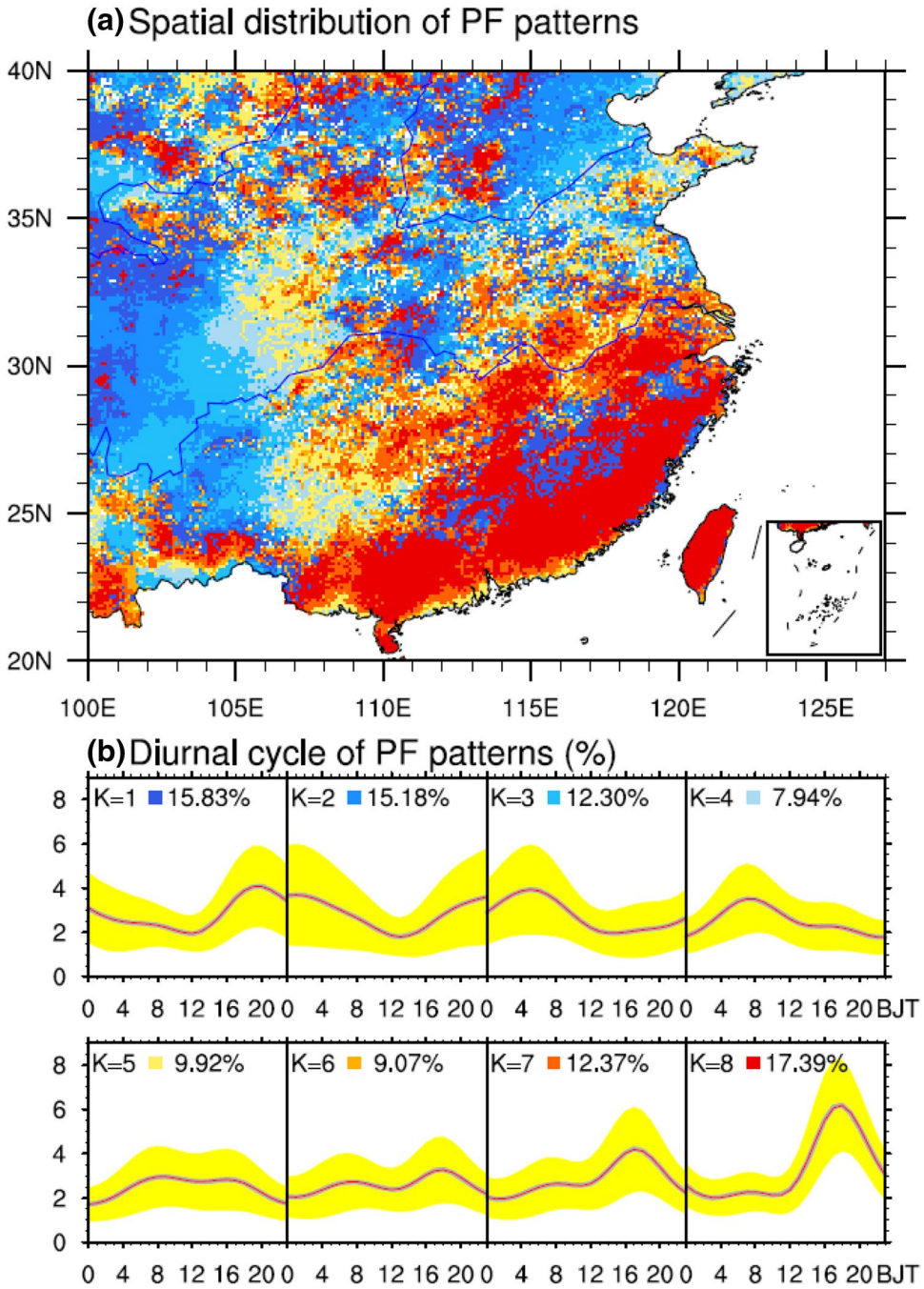

Fig. 8 Same as in Fig. 3, but for the PF with the duration time of 4–6 h

averaged every 3 h. From Fig. 10a–d, large 3-h mean rainfall with the intensity exceeding 0.4 mm h^{-1} during midnight to early morning is located over the south peripheries of Yungui Plateau and the eastern flanks of Tibetan Plateau. Specifically, large PA centers over the south peripheries of the Yungui Plateau develop gradually since 23:00 BJT, reach the maximal intensity above 0.6 mm h^{-1} during 02:00–07:00 BJT and then shift towards recession after 10:00 BJT. The maximal nocturnal rainfall can be explained by the enhanced warm-moist southerlies blowing against the Yungui and Tibetan Plateau (Fig. 10a), which carry more water vapor and interact with the local orographic convergence and ascending motions. Along the lee side of Tibetan Plateau, Sichuan Basin, Qinling-Wushan Mountains and the adjacent lowlands, the PA shows remarkable eastward propagation tendencies. This is consistent with the diurnal clockwise rotation of the occurrence time of long-duration PPA in Fig. 2 and the coherent eastward phase time delay of both total and long-duration rainfall between 26°N and 32°N revealed by the cluster analysis (Figs. 3, 4, 5, 6). Besides the above two large PA centers, there also exists a relatively weaker

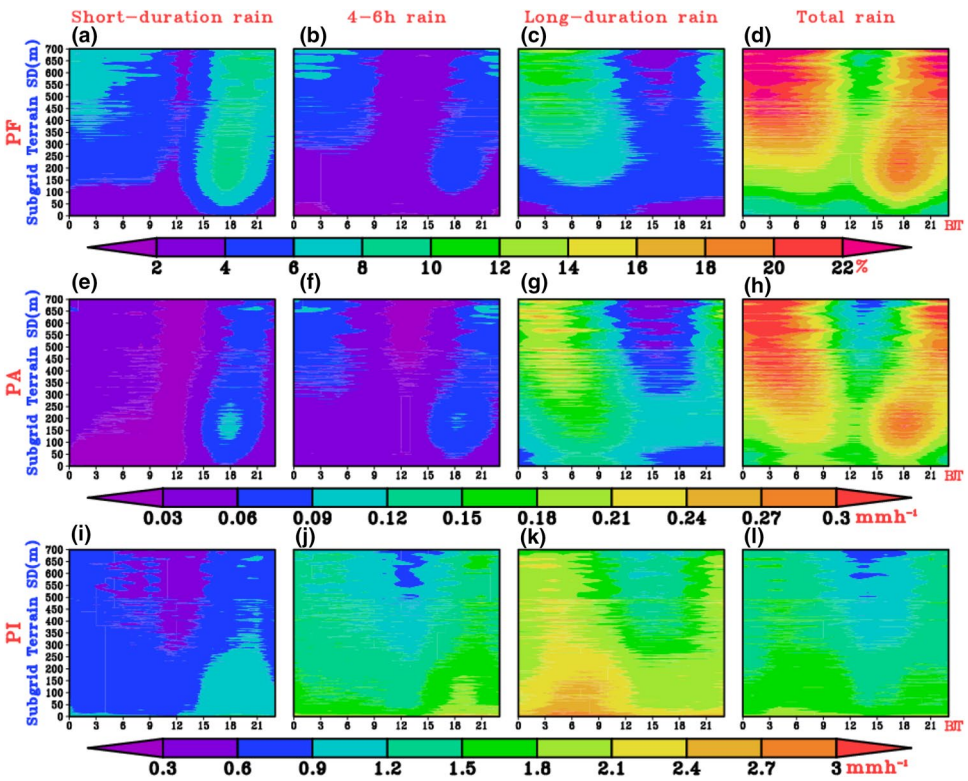

Fig. 9 The sub-grid terrain SD-time cross section of the hourly summer mean PA, PF and PI of the total, short-duration, 4–6 h and long-duration rainfall averaged over 2008–2014

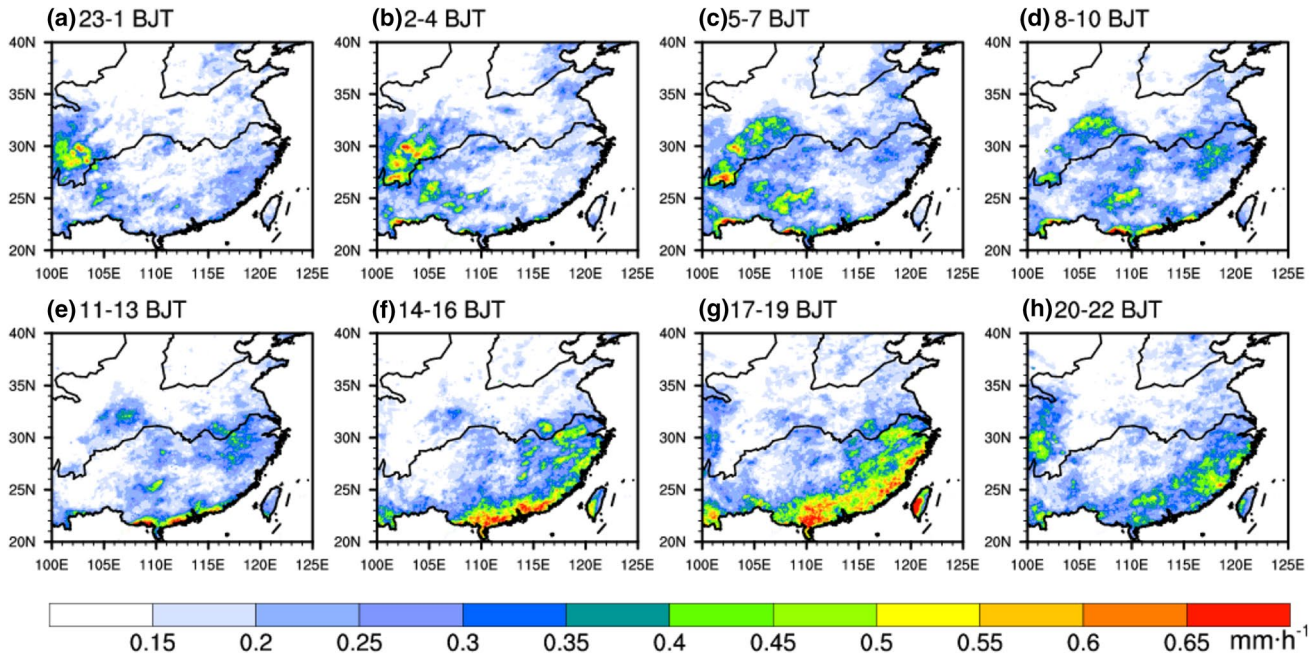

Fig. 10 Spatial distribution of the 3-h mean summer PA (mm) east to the Tibetan Plateau averaged over 2008–2014

midnight to morning (02:00–10:00 BJT) rainfall pattern over the middle-lower reaches of the Yangtze River Valley. Compared with the PA propagation in the eastern peripheries of Tibetan Plateau, the rainfall systems in the middle-lower reaches of the Yangtze River seem to begin developing locally since 02:00 BJT, accompanied by the initiation of the low-level convergence and the acceleration of the anomalous southwest moisture flux (Fig. 11a, b). Moreover, although the rainfall over the regions north to 35°N is below 0.2 mm h^{-1}, it can also be

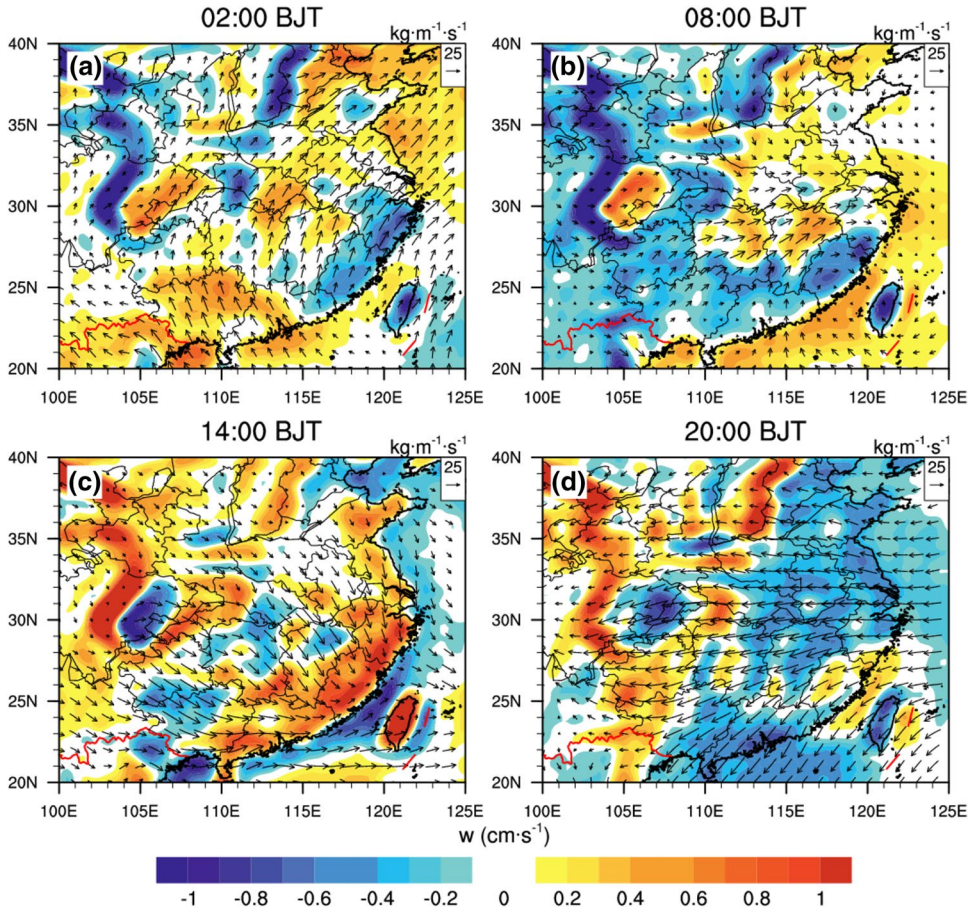

Fig. 11 Spatial distribution of the anomalous 850 hPa vertical motion (colored, cm s^{-1}) and the moisture flux (vectors, kg m^{-1} s^{-1}) vertically integrated from the ground surface to 300 hPa derived from the ERA Interim analyses at **a** 02:00, **b** 08:00, **c** 14:00, and **d** 20:00 BJT relative to the daily mean

noted that the rainfall over the Taihang Mountains during 17:00–22:00BJT prorogates southeastward to the downstream plains during 23:00–09:00 BJT.

As shown in Fig. 11, contrary to the atmospheric circulations at 02:00 BJT (Fig. 11a), the anomalous ascending motion centers at 14:00 BJT are located over the eastern slopes of the Tibetan Plateau, Yungui plateau, Qingling-Wushan Mountains, Taihang Mountains, southeastern hilly and coastal regions (Fig. 11c). Meanwhile, indicated by the northwestern moisture flux anomaly, the background southerly humidity fluxes are confined to southeastern hilly and coastal regions, which further lead to the PA maximal exceeding 0.5 mm h^{-1} between 14:00–19:00 BJT (Fig. 10f, g). At 20:00 BJT, the anomalous circulation is almost a complete reversal to that at 08:00 BJT due to the differential heating properties among the plateaus, highlands, plains and oceans, favoring afresh the late-evening to midnight rainfall formation on the eastern slopes of Tibetan Plateau and coastal regions.

3.3 Regional features of the diurnal variations of the precipitation with different duration time

Above results demonstrate that the diurnal variations of PA, PF and PI show distinct features over regions with contrasting terrain complexities such as plateaus vs. basins, mountains vs. valleys, and land vs. sea. Considering the similar step-like terrain and eastward-delayed diurnal phase of rainfall over the northern regions (35–40°N, 110–125°E) and southern regions (26–32°N, 110–125°E). Figures 12 and 13 further present the meridionally averaged sub-grid topography SD and the diurnal cycles of the PA for rainfall with different duration time along 100–125°E.

From Fig. 12, the short-duration rainfall over the land regions along 100–120°E displays intensively late-afternoon diurnal peaks (Fig. 12c), while the long-duration rainfall along 100–125°E shows prevailing midnight to morning diurnal peaks (Fig. 12e). The PA with the duration time of 4–6 h displays early-afternoon to early-evening peaks

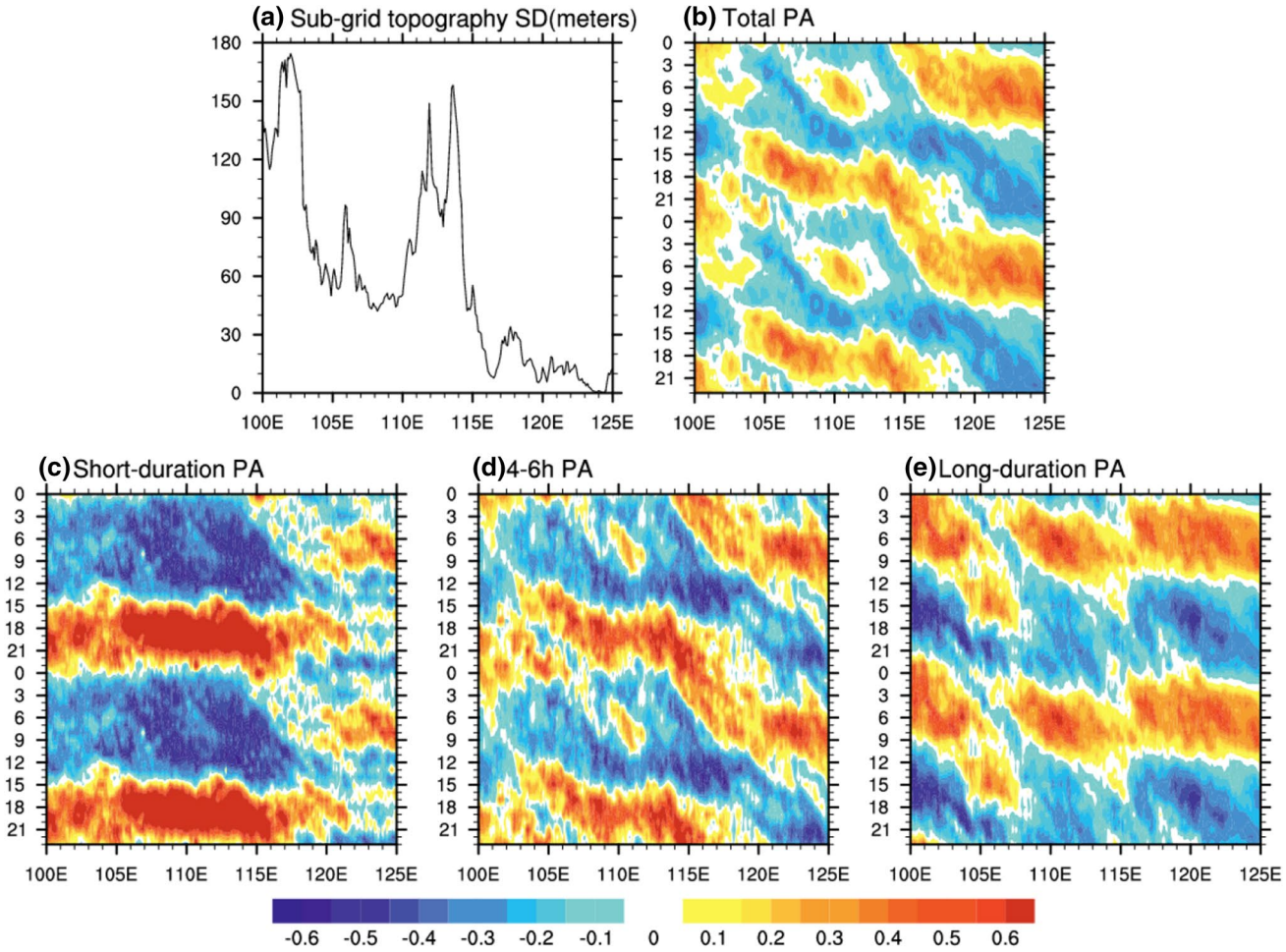

Fig. 12 **a** Sub-grid topography SD (m) and time-longitude cross section of the normalized diurnal variation of the 7-year (2008–2014) mean **a** total, **b** short-duration, **d** 4–6 h and **e** long-duration PA averaged along 35°N–40°N in summer

along 100–113°E and midnight to morning peaks along 113–125°E (Fig. 12d). The diurnal PA peaks of the total rainfall in Fig. 12b are determined by the relative strength among the diurnal PA peaks of the rainfall with different duration time. Overall, the PA of the total rainfall over the regions along 107–113°E displays two diurnal peaks (Fig. 12b). However, corresponding to the regions with relatively larger sub-grid terrain SD contrast in Fig. 12a, the PA of the total rainfall (Fig. 12b) tends to peak in midnight to morning (early evening to early morning) along 100–107°E (113–125°E). It is worth noting that the eastward-delayed diurnal phase of total rainfall during 00:00–09:00 BJT along the Tibetan Plateau to its downstream is closely related to the long-duration rainfall, while the eastward-delayed diurnal phase of total rainfall during 20:00–06:00 BJT along the Taihang mountains to North China Plain is mainly contributed by the rainfall with 4–6 h duration (Fig. 12b, d, e). As mentioned by a large number of previous studies, the enhanced nocturnal southwesterly, the mountain-plain solenoids and the coherent eastward migrating mesoscale convective systems may contribute to the eastward phase time delay of the PA diurnal cycle (Carbone et al. 2002; Tian et al. 2005; Jiang et al. 2006, 2017; Sun and Yang 2008; Chen et al. 2010; Huang et al. 2010a; Bao et al. 2011). However, the underlying processes still remain as an open question and the significant impact of 4–6 h rainfall on the eastward-delayed diurnal phase of total rainfall should be deeply revealed in the future work.

The southern parts of the study region exhibit great mountain-valley contrast between the Tibetan Plateau and Sichuan Basin, between Qinling-Wushan Mountains and the middle-lower reaches of Yangtze River Valley, and between the hilly areas and the ocean in the east (Fig. 1). Similar to the situations over the northern parts of the study region (Fig. 12c), the PA of the short-duration rainfall along 100–122°E mainly displays coherent late-afternoon diurnal peaks (Fig. 13c). The PA with the duration of 4–6 h presents an eastward phase time delay during 18:00–09:00

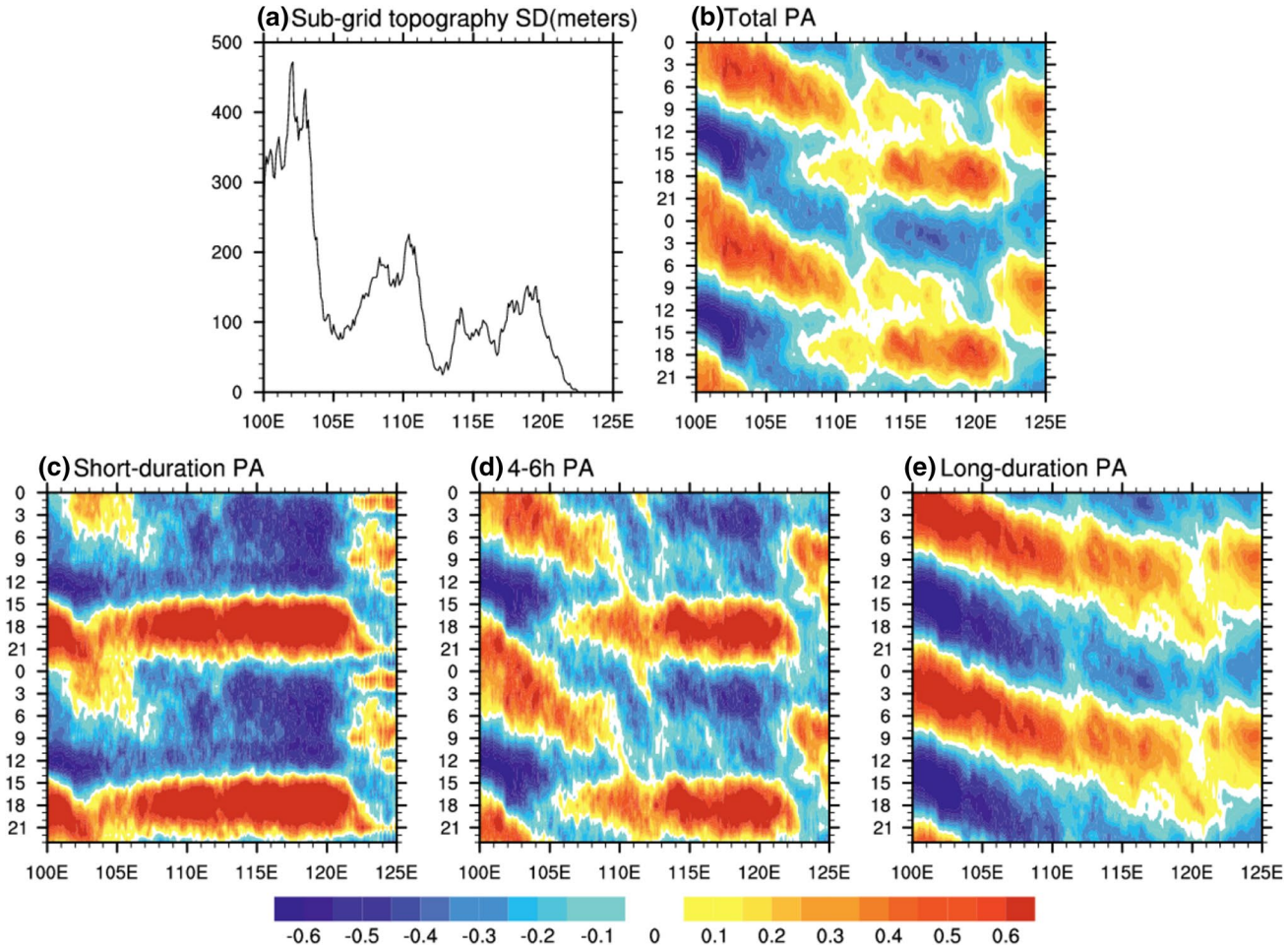

Fig. 13 **a** Sub-grid topography SD (m) and time-longitude cross section of the normalized diurnal variation of the 7-year (2008–2014) mean **a** total, **b** short-duration, **d** 4–6 h and **e** long-duration PA averaged along 26°N–32°N in summer

BJT along 100–106°E and a coherent late-afternoon peak over the regions between 100 and 122°E (Fig. 13d). However, the long-duration PA (as well as PF and PI, figures not shown) displays obvious eastward diurnal phase time delay during 00:00–18:00 BJT along 100–122°E, which contributed greatly to the eastward-delayed diurnal phase of total rainfall along the Tibetan Plateau to its downstream (Fig. 13b, e). In addition, compared to the faster eastward propagation speed of the total rainfall along the Tibetan Plateau to its downstream regions (100°E–110°E), the PA of the total rainfall over the regions between 110°E and 120°E with much smaller sub-grid terrain SD contrast (Fig. 13a) manifests a relatively slower propagation speed due to the meso-synoptic forcing associated with the monsoon system, such as the diurnal clockwise rotation of moisture fluxes related to the nocturnal accelerated low-level southwesterly jet in Fig. 11a, b (Chen et al. 2004, 2010; Wang et al. 2004; Ding and Chan 2005; Yuan et al. 2010).

Figures 12 and 13 vividly reveal the regional distributions of nocturnal, early-morning and late-afternoon rainfall patterns during summer. The short-duration rainfall usually peaks in late afternoon. The long-duration rainfall generally shows nocturnal or morning diurnal peaks. Over the eastern peripheries of the plateaus, the long-duration rainfall exhibits a similar propagation tendency to the total rainfall from late evening to morning. This may indicate the development, propagation and regeneration processes of convections with longer life cycles during summer (Carbone et al. 2002; Nesbitt and Zipser 2003; Wang et al. 2004; Jiang et al. 2006). On one hand, the thermal circulation caused by local mountain-valley thermal contrast may lead to the propagation of rainfall events over the regions downstream of the elevated regions, such as the Rocky Mountains, Tibetan Plateau and the Taihang Mountains (Koch et al. 2001; Carbone et al. 2002; He and Zhang 2010; Bao et al. 2011; Bao and Zhang 2013). On the other hand, large-scale monsoon systems, including the western Pacific subtropical high, the upper-level background westerlies, the low-level southwesterly jet and the Mei-yu front, also exert important modulating effects on the development of convection and

the corresponding eastward diurnal phase time delay. As revealed in Fig. 11a, b, the moisture transportation induced by the nocturnal southwesterly exhibits distinct diurnal variations. When coupled with the ascending motions provided by the mountain-plain solenoids, convective rainfall during midnight to early morning is easily triggered over North China Plain, Sichuan Basin and the middle-lower reaches of Yangtze River Valley (He and Zhang 2010; Huang et al. 2010a; Bao et al. 2011; Bao and Zhang 2013). During the active monsoon period, precipitation diurnal variations over the middle-lower Yangtze River Valley are characterized by the eastward phase time delay in the long-duration rainfall (Chen et al. 2010, 2012a; Yuan et al. 2010). Compared with the much faster eastward propagation speed along the eastern flanks of Tibetan Plateau to the downstream regions, the weaker solenoidal circulation associated with the weaker thermal contrast cannot adequately explain the much slower eastward propagation speed along Wushan Mountains to the downstream low-lying plains in Fig. 13b, e. However, it is worth noting that the southwesterly moisture transportation during 02:00–08:00 BJT exhibits a diurnal clockwise rotation and enhancement process over the middle-lower Yangtze River Valley (Fig. 11a, b). The warm and moist flow will further converge and rise along the Mei-yu front therein, leading to the formation and propagation of long-lived meso-scale convective rainfall in the warmer frontal regions (Chen et al. 2004, 2012a; Wang et al. 2004; Geng and Yamada 2007; Sun and Zhang 2012; Luo et al. 2014).

As discussed by Bao et al. (2011), the mountain-plain solenoids initially triggered by differential heating between complex terrains play an important role in the rainfall evolution over the regions east to Tibetan Plateau. Focused on the southern areas along 26–32°N, the meridionally averaged deviations of the vertical motion, circulations and meridional winds relative to the daily mean, and the corresponding normalized diurnal PA with different duration time are shown in Fig. 14. At 02:00 BJT, due to the mountain-valley and land–ocean thermal contrast, there exist three anomalous ascending motions located over Sichuan Basin, Yangtze River Valley and ocean. Meanwhile, the abundant moisture fluxes carried by the nocturnal accelerated southwesterly (Fig. 11a) lead to the increases of atmospheric precipitable water and relative humidity, which favors the formation and development of the midnight to early-morning convective systems over there. As a result, the total and long-duration rainfall (purple and green lines in Fig. 14a, respectively) show large normalized deviations of PA over the Sichuan Basin where the anomalous ascending motion is especially strong due to the largest mountain-valley thermal contrast.

Indicated by the stronger positive anomaly of meridional wind at 08:00 BJT (Fig. 14b), the low-level southwesterly jet exhibits an enhancement process over the middle-lower reaches of Yangtze River Valley due to the nighttime decrease of boundary friction and turbulence diffusion over flatlands (Chen et al. 2010; Bao et al. 2011). As revealed in Fig. 11b, the regions with strong water vapor transport shifted to the regions east to 110°E, corresponding to the diurnal clockwise rotation of the anomalous low-tropospheric monsoon circulation. Collocated with the lifting effect of the mountain-plain solenoid's upward branch widely spreading along 112–118°E (Fig. 14b) and the strong quasi-stationary Mei-yu front (Wang et al. 2004; Chen et al. 2012a; Luo et al. 2014), the long-duration rainfall with a relatively larger diurnal normalized deviation around 0.4 is widely distributed over the middle-lower reaches of Yangtze River Valley. Meanwhile, the short-duration rainfall at 02:00 and 08:00 BJT (pink lines in Fig. 14a, b) is largely suppressed and can only be caught by a weak signal over ocean.

Contrary to the nocturnal circulations at 02:00 BJT (Fig. 14a), the upward branches of the mountain-plain solenoids move to the plateau-highland slopes, hilly and coastal regions at 14:00 BJT (Fig. 14c). In addition, the daytime anomalous northerlies and northwesterly moisture fluxes are also reversals of the nighttime situation (Fig. 14c vs. a, Fig. 11c vs. a). Consequently, the rainfall is substantially suppressed at 14:00 BJT and there only exists a low PPA around 118°E due to the strong local thermal convections. The normalized diurnal deviation of the short-duration rainfall at 14:00 BJT over the southeastern hilly regions increases with the development of thermal convections compared with that at 02:00 and 08:00 BJT (Fig. 14a, b), indicating the following intensive outbreak of short-duration rainfall during 15:00–19:00 BJT depicted in Fig. 10f, g when the ERA Interim data is not available.

The strong large-scale mountain-plain solenoid circulation with the upward branch over the eastern slopes of the Tibetan Plateau and the sinking branch over the lowlands and ocean at 20:00 BJT (Fig. 14d) is a reversal of the situation at 08:00 BJT in Fig. 14b. The large-scale anomalous descending motions dominate the regions between 110 and 120°E and further suppress the long-duration precipitation. However, in the coastal areas east to 120°E, the early-evening PPA for the total, short-duration, and long-duration rainfall can be ascribed to the favorable thermal dynamical conditions provided by the anomalous upward motion and the water vapor transport associated with the sea breeze. Due to the abundant warm-moist air from the low-lying basins, the short-duration rainfall is extensively distributed over the east slopes of Tibetan Plateau until the anomalous circulation reverses at 02:00 BJT (Figs. 11a, 14a).

4 Summary and discussion

In this study, the satellite-gauge merged precipitation product at 1-h interval and 0.1° latitude by 0.1° longitude grid spacing during 2008–2014 is utilized to systematically reveal the diurnal characteristics of summer

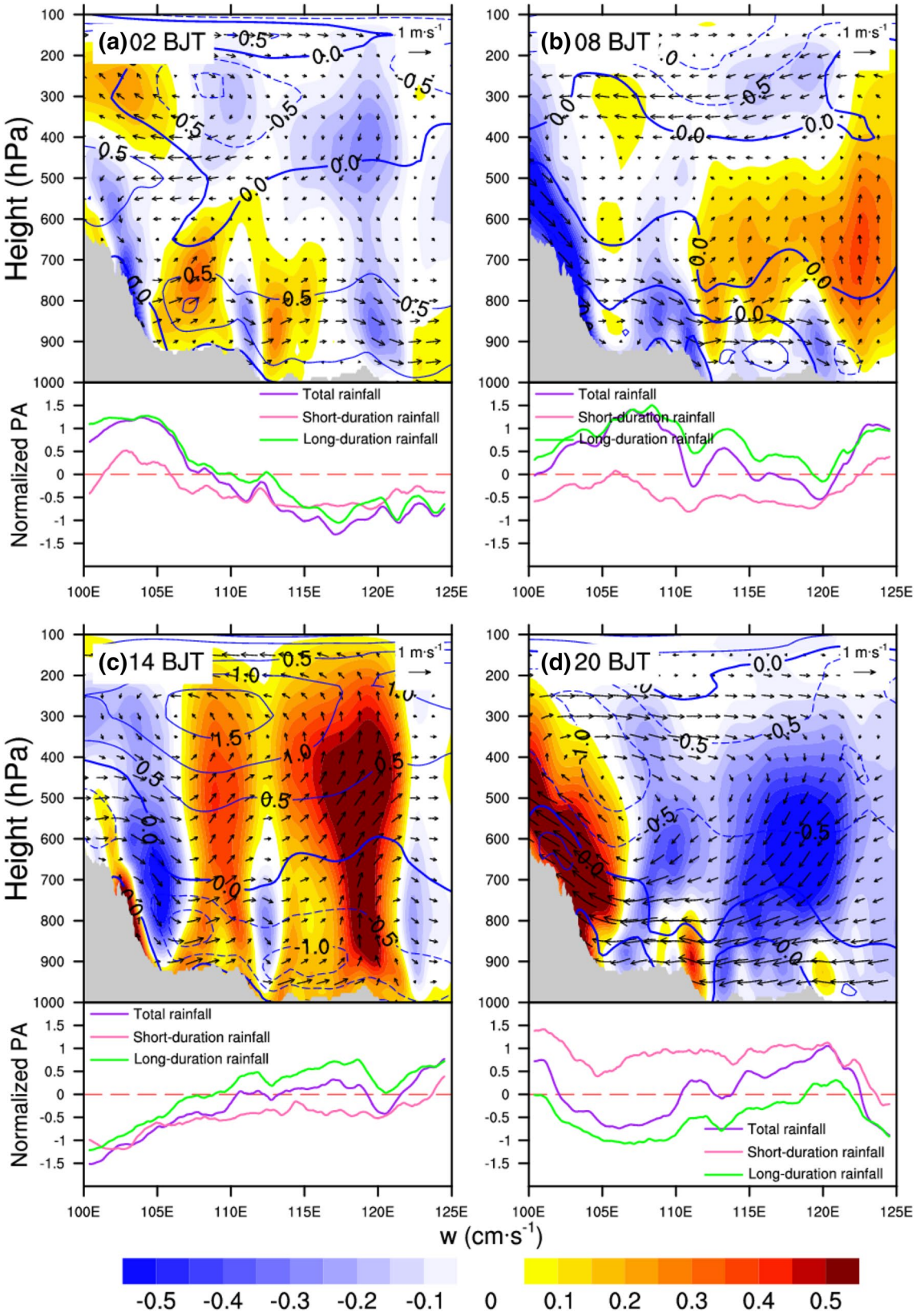

Fig. 14 Height-longitude cross section of the 7-year (2008–2014) summer averaged vertical motion (shaded, cm s^{-1}), the vertical circulation vectors (zonal winds and 100 times of vertical velocity) and the meridional winds (contours, m s^{-1}; solid blue, positive; dashed, negative) deviations relative to the daily mean from the ERA Interim data, and the normalized PA diurnal cycles averaged along 26°N–32°N at **a** 02:00, **b** 08:00, **c** 14:00, and **d** 20:00 BJT. The gray areas denote the terrain height avraged along 26°N–32°N

precipitation over the regions east to the Tibetan Plateau. The major findings are summarized as follows:

The PPA, PPF and PPI of the total, short-duration and long-duration rainfall show distinct regional differences over eastern China during summer. In general, large PPA and PPF of the total rainfall mainly locate over the southern peripheries of Yungui Plateau, eastern flanks of Tibetan Plateau, Qinling-Wushan Mountains, and southeastern hilly and coastal regions. Differently, relatively strong PPI happens easily in Sichuan Basin, middle-lower reaches of the Yangtze River Valley, North China Plain and coastal plains in southern China. The PA and PF of the short-duration rainfall show coherent late-afternoon peaks over the elevated mountain ranges, southeastern hilly and coastal regions, while the large PPI only locates over the North China Plain. The long-duration rainfall is the major contributor to the total rainfall over most parts of the study region. Moreover, the PPA, PPF and PPI of the long-duration rainfall consistently exhibit a diurnal clockwise rotation from the eastern plateau slopes to the middle-lower reaches of Yangtze River Valley.

Eight typical diurnal patterns of the PA, PF and PI in summer identified by the cluster analysis further show obvious regional features among the plateaus, basins, plains, hilly and coastal regions. The PA of total rainfall displays late-afternoon patterns over Loess Plateau, southeastern hilly and coastal regions, early-evening patterns over the Tibetan Plateau and Taihang Mountains, and the midnight to early-morning patterns over the downstream basins or plains of the elevated regions. Over the regions along the elevated Tibetan Plateau and Taihang mountains to their downstream lowlands, the PA diurnal patterns of the total rainfall shows an apparent eastward phase time delay during 22:00–08:00 BJT. These regional-scale differences and eastward phase time delay in the total rainfall are much clearer in the cluster results of PF. All of the eight typical PF diurnal patterns in the short-duration rainfall show a leading late-afternoon diurnal peak. The long-duration PF patterns with midnight to early-morning peaks are widely distributed over the areas east to Tibetan and Yungui Plateaus between 100 and 110°E, meanwhile, a relatively weak late-afternoon diurnal peak of the long-duration PF can be found over the Loess Plateau, Taihang mountains, Qinling-wushan mountains and southeastern hilly and coastal regions.

Additionally, the analysis of the relations between precipitation diurnal cycles and sub-grid terrain SD indicate that precipitation diurnal variations over the regions east to Tibetan Plateau are significantly affected by the sub-grid topography fluctuations. The PA, PF and PI of the total rainfall display much more pronounced diurnal peaks with the sub-grid topography SD decreased. Meanwhile, with the sub-grid topography SD increased, the diurnal peaks of the PA and PF (PI) for the rainfall with different duration time strengthen (weaken).

The diurnal cycles of the total rainfall over most eastern China exhibit eastward phase time delay. The eastward-delayed diurnal phase of the total rainfall along the Tibetan Plateau to its downstream is mainly due to the long-duration (> 6 h) rainfall. However, the eastward-delayed diurnal phase of the total rainfall along the Taihang Mountains to North China Plain is mainly contributed by the rainfall with 4–6 h duration. Further mechanism analysis indicates that the eastward phase time delay of the long-duration rainfall is closely related to the diurnal variations of the upward branches of thermally driven mountain-plain solenoids and the moisture fluxes carried by the accelerated nocturnal southwesterly winds. The late-afternoon peaks of the short-duration rainfall occur intensively over the southeastern hilly and coastal regions due to the strong local thermal convections. However, the early-evening peaks of the short-duration rainfall over the elevated mountain ranges are significantly affected by the upward warm-moist wind from the surrounding low-lying basins and plains.

At present, we merely consider the comprehensive impacts of the local topography and large-scale circulations on the diurnal variations of the total, short-duration and long-duration rainfall during summer. In fact, the intraseasonal movements of the summer monsoon systems, including the position and strength of western Pacific subtropical high, the associating variations of the tropospheric upper-level jet streams, and the corresponding prevailing winds at lower troposphere, also exert great impacts on the diurnal precipitation features (Ding and Chan 2005; Geng and Yamada 2007; Chen et al. 2009a, b; Yin et al. 2009; Yuan et al. 2010; Jiang et al. 2017). Therefore, future studies should focus on examining the combined effect of complex topography and monsoon climate in modulating the precipitation diurnal variability by using much higher spatiotemporal resolution data and numerical simulations.

Acknowledgements This work was supported by the National Natural Science Foundation of China under Grants (91537102, 91637107), Opening Fund of Key Laboratory of Land Surface Process and Climate Change in Cold and Arid Regions, Chinese Academy of Sciences (LPCC201502), the Jiangsu University "Blue Project" outstanding young teachers training object, the Fundamental Research Funds for the Central Universities and the Jiangsu Collaborative Innovation Center for Climate Change. We are grateful to United State Geological Survey (https://lta.cr.usgs.gov/GTOPO30) and ECMWF (http://apps.ecmwf.int/datasets/data/interim-full-daily/) for allowing us to use the GTOPO 30 s and ERA Interim data. We thank National Meteorological Information Administration of China for providing the gauge-satellite merged precipitation data. The authors acknowledge the Editor and three anonymous reviewers for the careful review and constructive comments.

References

Angelis CF, Mcgregor GR, Kidd C (2004) Diurnal cycle of rainfall over the Amazon basin. Clim Res 26(2):139–149. https://doi.org/10.3354/cr026139

Bao X, Zhang F (2013) Impacts of the mountain-plains solenoid and cold pool dynamics on the diurnal variation of warm-season precipitation over northern China. Atmos Chem Phys 13:6965–6982. https://doi.org/10.5194/acpd-12-27891-2012

Bao X, Zhang F, Sun J (2011) Diurnal variations of warm-season precipitation east of the Tibetan Plateau over China. Mon Weather Rev 139(9):2790–2810. https://doi.org/10.1175/MWR-D-11-00006.1

Benedetto JJ (1996) Harmonic analysis and applications (studies in advanced mathematics). CRC Press, Boca Raton

Betts AK, Jakob C (2002) Study of diurnal cycle of convective precipitation over Amazonia using a single column model. J Geophys Res 107(D23):ACL 25-1–ACL 25-13. https://doi.org/10.1029/2002JD002264

Carbone RE, Tuttle JD (2008) Rainfall occurrence in the US warm season: the diurnal cycle. J Clim 21(16):4132–4146. https://doi.org/10.1175/2008JCLI2275.1

Carbone RE, Tuttle JD, Ahijevych DA, Trier SB (2002) Inferences of predictability associated with warm season precipitation episodes. J Atmos Sci 59(13):2033–2056

Chen Y, Li J (1995) Large-scale conditions favorable for the development of heavy rainfall during TAMEX-IOP-3. Mon Weather Rev 123(10):2978–3002. https://doi.org/10.1175/1520-0493(1995)123<2978:LSCFFT>2.0.CO;2

Chen T, Wang S, Huang W, Yen M (2004) Variation of the East Asian summer monsoon rainfall. J Clim 17(4):744–762. https://doi.org/10.1175/1520-0442(2004)017<0744:VOTEAS>2.0.CO

Chen G, Sha W, Iwasaki T (2009a) Diurnal variation of precipitation over southeastern China: 2. Impact of the diurnal monsoon variability. J Geophys Res 114(D21):6149–6150. https://doi.org/10.1029/2009JD012181

Chen G, Sha W, Iwasaki T (2009b) Diurnal variation of precipitation over southeastern China: spatial distribution and its seasonality. J Geophys Res 114(D13):267–275. https://doi.org/10.1029/2008JD011103

Chen H, Yu R, Li J, Yuan W, Zhou T (2010) Why nocturnal long-duration rainfall presents an eastward-delayed diurnal phase of rainfall down the Yangtze River Valley. J Clim 23(4):905–917. https://doi.org/10.1175/2009JCLI3187.1

Chen G, Sha W, Iwasaki T, Ueno K (2012a) Diurnal variation of rainfall in the Yangtze River Valley during the spring-summer transition from TRMM measurements. J Geophys Res 117:D06106. https://doi.org/10.1029/2011JD017056

Chen H, Yuan W, Li J, Yu R (2012b) A possible cause for different diurnal variations of warm season rainfall as shown in station observations and TRMM 3B42 data over the southeastern Tibetan Plateau. Adv Atmos Sci 29(1):193–200. https://doi.org/10.1007/s00376-011-0218-1

Chen G, Sha W, Sawada M, Iwasaki T (2013) Influence of summer monsoon diurnal cycle on moisture transport and precipitation over eastern China. J Geophys Res 118(8):3163–3177. https://doi.org/10.1002/jgrd.50337

Chen X, Zhao K, Xue M (2014) Spatial and temporal characteristics of warm season convection over Pearl River Delta region, China, based on 3 years of operational radar data. J Geophys Res 119:12,447–12,465. https://doi.org/10.1002/2014JD021965

Dai A, Trenberth KE (2004) The diurnal cycle and its depiction in the community climate system model. J Clim 17(5):930–951. https://doi.org/10.1175/1520-0442(2004)017<0930:TDCAID>2.0.CO;2

Dai A, Giorgi F, Trenberth KE (1999) Observed and model-simulated diurnal cycles of precipitation over the contiguous United States. J Geophys Res 104(D6):6377–6402. https://doi.org/10.1029/98JD02720

DeMott CA, Randall DA, Khairoutdinov M (2007) Convective precipitation variability as a tool for general circulation model analysis. J Clim 20(1):10–1175. https://doi.org/10.1175/JCLI3991.1

Ding Y, Chan J (2005) The East Asian summer monsoon: an overview. Meteorol Atmos Phys 89(1):117–142. https://doi.org/10.1007/s00703-005-0125-z

Ding Y, Zhang Y, Ma Q, Hu Q (2001) Analysis of the large-scale circulation features and synoptic system in East Asia during the intensive observation period of GAME/HUBEX. J Meteorol Soc Jpn 79(1B):277–300

Fujibe F (1989) Short-term precipitation patterns in central Honshu, Japan. Classification with the fuzzy c-means method. J Meteorol Soc Jpn 67(6):967–983

Fujibe F (1999) Diurnal variation in the frequency of heavy precipitation in Japan. J Meteorol Soc Jpn 77(6):1137–1149

Geng B, Yamada H (2007) Diurnal variations of the meiyu/baiu rain belt. Sci Online Lett Atmos Sola 3(263):61–64. https://doi.org/10.2151/sola.2007-016

He H, Zhang F (2010) Diurnal variations of warm-season precipitation over Northern China. Mon Weather Rev 138(4):1017–1025. https://doi.org/10.1175/2010MWR3356.1

Higgins R, Yao Y, Yarosh E, Janowiak J, Mo K (1997) Influence of the Great Plains low-level jet on summertime precipitation and moisture transport over the central United States. J Clim 10:481–507. https://doi.org/10.1175/1520-0442(1997)010<0481:IOTGPL>2.0.CO;2

Hirose M, Nakamura K (2005) Spatial and diurnal variation of precipitation systems over Asia observed by the TRMM precipitation radar. J Geophys Res 110(D5):781–797. https://doi.org/10.1029/2004JD004815

Huang H, Wang C, Chen T, Carbone RE (2010a) The role of diurnal solenoidal circulation on propagating rainfall episodes near the eastern Tibetan Plateau. Mon Weather Rev 138(7):2975–2989. https://doi.org/10.1175/2010MWR3225.1

Huang W, Chan J, Wang S (2010b) A planetary-scale land-sea breeze circulation in East Asia and the western North Pacific. Q J R Meteor Soc 136(651):1543–1553. https://doi.org/10.1002/qj.663

Jiang X, Lau N, Klein SA (2006) Role of eastward propagating convection systems in the diurnal cycle and seasonal mean of summertime rainfall over the US Great Plains. Geophys Res Let 33(33):277–305. https://doi.org/10.1029/2006GL027022

Jiang Z, Zhang D, Xia R, Qian T (2017) Diurnal variations of presummer rainfall over Southern China. J Clim 30:755–773. https://doi.org/10.1175/JCLI-D-15-0666.1

Joyce R, Janowiak JE, Arkin PA, Xie P (2004) CMORPH: a method that produces global precipitation estimates from passive microwave and infrared data at high spatial and temporal resolution. J Hydrometeorol 5(3):287–296. https://doi.org/10.1175/1525-7541(2004)005<0487:CAMTPG>2.0.CO;2

Koch SE, Zhang F, Kaplan ML (2001) Numerical simulations of a gravity wave event over CCOPE. Part III: the role of a mountain plains solenoid in the generation of the second wave episode. Mon Weather Rev 129(5):909–933. https://doi.org/10.1175/1520-0493(2001)129<0909:NSOAGW>2.0.CO;2

Li Y, Yu R, Xu Y (2004) Spatial distribution and seasonal variation of cloud over China based on ISCCP Data and surface observations. J Meteorol Soc Jpn 82(2):761–773. https://doi.org/10.2151/jmsj.2004.761

Li J, Yu R, Zhou T (2008) Seasonal variation of the diurnal cycle of rainfall in the southern contiguous China. Biochem Biophys Res Commun 21(22):277–287. https://doi.org/10.1175/2008JCLI2188.1

Lin X, Randall DA, Fowler LD (2000) Diurnal variability of the hydrological cycle and radiative fluxes: comparisons between observations and a GCM. J Clim 13(23):4159–4179. https://doi.org/10.1175/1520-0442(2000)013<4159:DVOTHC>2.0.CO;2

Luo Y, Wang H, Zhang R, Qian W, Luo Z (2013) Comparison of rainfall characteristics and convective properties of monsoon precipitation systems over South China and the Yangtze and Huai River Basin. J Clim 26:110–132. https://doi.org/10.1175/JCLI-D-12-00100.1

Luo Y, Gong Y, Zhang D (2014) Initiation and organizational modes of an extreme-rain-producing mesoscale convective system along a Mei-Yu front in east China. Mon Weather Rev 142:203–221. https://doi.org/10.1175/MWR-D-13-00111.1

Nesbitt SW, Zipser EJ (2003) The diurnal cycle of rainfall and convective intensity according to three years of TRMM measurements. J Clim 16(10):1456–1475. https://doi.org/10.1175/1520-0442-16.10.1456

Pan Y, Shen Y, Yu J, Zhao P (2012) Analysis of the combined gauge-satellite hourly precipitation over China based on the OI technique. Acta Meteorol Sin 70(6):1381–1389

Roy SS, Balling RC (2005) Analysis of diurnal patterns in winter precipitation across the conterminous United States. Mon Weather Rev 133(133):707–711. https://doi.org/10.1175/MWR-2873.1

Shen Y, Pan Y, Yu J, Zhao P, Zhou Z (2013) Quality assessment of hourly merged precipitation product over China. Trans Atmos Sci 36(1):37–46

Shen Y, Zhao P, Pan Y, Yu J (2014) A high spatiotemporal gauge-satellite merged precipitation nanalysis over China. J Geophys Res 119:3063–3075. https://doi.org/10.1002/2013JD020686

Sorooshain S, Maddox RA, Gao X, Gupta HV (2002) Diurnal variability of tropical rainfall retrieved from combined GOES and TRMM satellite information. J Clim 15(9):983–1001. https://doi.org/10.1175/1520-0442(2002)015<0983:DVOTRR>2.0.CO;2

Sun J, Yang B (2008) Meso-β scale torrential rain affected by topography and the urban circulation. Chin J Atmos Sci 32(6):1352–1364

Sun J, Zhang F (2012) Impacts of mountain–plains solenoid on diurnal variations of rainfalls along the Mei-Yu front over the East China Plains. Mon Weather Rev 140:379–397. https://doi.org/10.1175/MWR-D-11-00041.1

Tian B, Held IM, Lau NC, Soden BJ (2005) Diurnal cycle of summertime deep convection over North America: a satellite perspective. J Geophys Res 110(D08). https://doi.org/10.1029/2004JD005275

Wang W, Gong W, Wei H (2000) A regional model simulation of the 1991 severe precipitation event over the Yangtze-Huai River Valley. Part I: precipitation and circulation statistics. J Clim 13(1):74–92. https://doi.org/10.1175/1520-0442(2000)013<0093:ARMSOT>2.0.CO;2

Wang C, Chen G, Carbone RE (2004) A climatology of warm-season cloud patterns over therEast Asia based on GMS infrared brightness temperature observations. Mon Weather Rev 132:1606–1629. https://doi.org/10.1175/1520-0493

Wu G, Liu Y, Zhang Q, Wan R, Duan A, Wang T, Liu X, Li W, Wang Z, Liang X (2007) The influence of mechanical and thermal forcing by the Tibetan Plateau on Asian climate. J Hydrometeor 8(4):770–789. https://doi.org/10.1175/JHM609.1

Xie S, Xu H, Saji NH, Wang Y, Liu WT (2006) Role of narrow mountains in large-scale organization of Asian monsoon convection. J Clim 19:3420–3429. https://doi.org/10.1175/JCLI3777.1

Xu W, Zipser EJ (2011) Diurnal variations of precipitation, deep convection, and lightning over and east of the eastern Tibetan Plateau. J Clim 24(24):448–465. https://doi.org/10.1175/2010JCLI3719.1

Yang S, Smith EA (2005) Mechanisms for diurnal variability of global tropical rainfall observed from TRMM. J Clim 19(20):5190–5226. https://doi.org/10.1175/JCLI3883.1

Yin S, Chen D, Xie Y (2009) Diurnal variations of precipitation during the warm season over China. Int J Climatol 29(8):1154–1170. https://doi.org/10.1002/joc.1758

Yu R, Zhou T, Xiong A, Zhu Y, Li J (2007a) Diurnal variations of summer precipitation over contiguous China. Geophys Res Lett 34(1):223–234. https://doi.org/10.1029/2006GL028129

Yu R, Xu Y, Zhou T, Li J (2007b) Relation between rainfall duration and diurnal variation in the warm season precipitation over central eastern China. Geophys Res Lett 34(13):173–180. https://doi.org/10.1029/2007GL030315

Yu R, Li J, Chen H (2009) Diurnal variation of surface wind over central eastern China. Clim Dyn 33(7–8):1089–1097. https://doi.org/10.1007/s00382-008-0478-3

Yu J, Shen Y, Pan Y, Zhao P, Zhou Z (2013) Improvement of satellite-based precipitation estimates over China based on probability density function matching method. J Appl Meteorol 24(5):544–553

Yu R, Li J, Chen H, Yuan W (2014) Progress in studies of the precipitation diurnal variation over contiguous China. Acta Meteorol Sin 72(5):948–968

Yuan W, Yu R, Chen H, Li J, Zhang M (2010) Subseasonal characteristics of diurnal variation in summer monsoon rainfall over central eastern China. J Clim 23(24):6684–6695. https://doi.org/10.1175/2010JCLI3805.1

Yuan W, Yu R, Zhang M, Lin W, Chen H, Li J (2012) Regimes of diurnal variation of summer rainfall over subtropical East Asia. J Clim 25(9):3307–3320. https://doi.org/10.1175/JCLI-D-11-00288.1

Yuan W, Yu R, Fu Y (2014a) Study of different diurnal variations of summer long-duration rainfall between the southern and northern parts of the Huai River. Chin J Geophys 57(57):286–287. https://doi.org/10.1002/cjg2.20092

Yuan W, Sun W, Chen H, Yu R (2014b) Topographic effects on spatiotemporal variations of short-duration rainfall events in warm season of central North China. J Geophys Res 119(19):223–234. https://doi.org/10.1002/2014JD022073

Zhang W, Huang A, Zhou Y, Yang B, Fang D, Zhang L, Wu Y (2017) Diurnal cycle of precipitation over Fujian Province during the pre-summer rainy season in southern China. Theor Appl Climatol. https://doi.org/10.1007/s00704-016-1927-2

Zhou T, Yu R, Chen H, Dai A, Pan Y (2008) Summer precipitation frequency, intensity, and diurnal cycle over China: a comparison of satellite data with gauge observations. J Clim 21(2007):3997–4010. https://doi.org/10.1175/2008JCLI2028SI

Zhuo H, Zhao P, Zhou T (2014). Diurnal cycle of summer rainfall in Shandong of eastern China. Int J Climatol 34(3):742–750. https://doi.org/10.1002/joc.3718